Numerical investigation of a model for oxygen ordering in $YBa_2Cu_3O_{6+x}$

T. Aukrust
IBM Bergen Scientific Centre, Thormøhlensgate 55, Bergen High Technology Centre, N-5008 Bergen, Norway

M. A. Novotny*
Supercomputer Computations Research Institute B-186, Florida State University, Tallahassee, Florida 32306-4052

P. A. Rikvold
Department of Physics B-159, Center for Materials Research and Technology B-159, and Supercomputer Computations Research Institute B-186, Florida State University, Tallahassee, Florida 32306-3016

D. P. Landau
Department of Physics and Astronomy and Center for Simulational Physics, University of Georgia, Athens, Georgia, 30602
(Received November 7, 1989)

We report the results of large-scale Monte Carlo and transfer-matrix studies of a model lattice-gas Hamiltonian that has previously been introduced to study the oxygen ordering responsible for the orthorhombic-to-tetragonal transition in $YBa_2Cu_3O_{6+x}$. We analyze the data using finite-size scaling to obtain the phase diagram and critical exponents. At high temperatures we find qualitative agreement with the cluster-variation method. However, at low temperatures we find only second-order transitions, in disagreement with the cluster-variation method. The critical exponents found are consistent with the universality classes of the $d=2$ Ising model and the XY model with cubic anisotropy. Consequently, any experimental evidence of a first-order transition for $YBa_2Cu_3O_{6+x}$ would imply that the model of Wille *et al.* [Phys. Rev. Lett. **60**, 1065 (1988)] needs to be modified to be directly applicable to this material.

I. INTRODUCTION

With the discovery of the first high-temperature superconductors[1] and of superconductivity above liquid-nitrogen temperatures[2] in the copper-oxide based ceramics $R Ba_2Cu_3O_{6+x}$ (where R is a rare-earth element and $\frac{1}{2} \lesssim x < 1$) possibilities of widespread commercial applications of superconductivity have emerged.[3] However, before commercial uses of these materials can be developed, reliable techniques are needed for large-scale manufacturing. The oxygen content is one important aspect that must be understood before this goal can be accomplished.

Since the temperature at which the superconducting transition takes place depends critically on the oxygen concentration,[4-7] it is important to understand the phase diagram for the oxygen ordering that occurs in the copper-oxide basal planes. If the oxygen content is low ($x < \frac{1}{2}$) the material has a tetragonal phase and is not superconducting, whereas if $\frac{1}{2} \lesssim x < 1$ the superconducting properties can depend critically on the oxygen ordering, as well as on the oxygen stoichiometry. Thus the ceramic with $x = \frac{1}{2}$ and with yttrium as the rare earth has a tetragonal phase obtained by rapid quenching from high temperatures and a superconducting temperature near 0 K, whereas the material with the same oxygen concentration, but obtained with a gettering technique, has an orthorhombic structure and a superconducting transition of about 60 K.[5] At larger O concentrations, $x \sim 1$, the material is orthorhombic and has a superconducting transition near 90 K. The experimental evidence for both the tetragonal and orthorhombic phases comes from x-ray[5,8] and neutron studies,[4,9] as well as electron diffraction and microscopy.[6,10,11] In both the orthorhombic phases, the basal Cu-O planes have been found to contain parallel chains of O atoms.

When oxygen chains form in the basal planes of the $R Ba_2Cu_3O_{6+x}$ materials, the symmetry between the two axes of the planes is broken. For this reason theoretical models for the high-temperature tetragonal to orthorhombic transition in $R Ba_2Cu_3O_{6+x}$ have assumed that the chain formation drives the transition. Most theoretical treatments have assumed that the relevant physics is contained solely in the basal planes,[12-18] although Khachaturyan *et al.*[19-21] have argued that, to correctly describe the ordering process, the full three-dimensional nature of the materials must be used.

Lattice-gas models can be constructed that reproduce the experimentally observed structures of $R Ba_2Cu_3O_{6+x}$. These are the tetragonal phase with $x \approx 0$, the orthorhombic structure with $x \approx 1$, and the orthorhombic "double-cell" phase, which has $x \approx \frac{1}{2}$.[5,8] In addition, the nature of the transitions in the lattice-gas model (whether the transitions are first order or contin-

uous) should correspond to the nature of the experimentally observed transitions.

In this paper we study the two-dimensional lattice-gas Hamiltonian, which was introduced by Wille *et al.*[12,18,22–24] for the oxygen ordering in the basal planes of $YBa_2Cu_3O_{6+x}$. We investigate this model using both transfer-matrix and Monte Carlo, techniques. The relevance of this particular model to the physical materials has recently been reviewed.[25,26] Previous studies of this model have used the cluster-variation method.[18,27] However, it is important to fully understand the phase diagram obtained from this model through nonperturbative methods such as Monte Carlo and transfer-matrix techniques, so that an accurate comparison to experimental data can be made. In this paper we have concentrated on the critical properties, both the phase diagram and critical exponents, of the model with the goal of comparing the results obtained from transfer-matrix, Monte Carlo, and cluster-variation methods. Recent independent work has applied transfer-matrix methods[28] and Monte Carlo methods (without obtaining the critical exponents)[29,30] to this model.

In Sec. II we describe the lattice-gas model and its relevant ground states. In Sec. III we give the details of our Monte Carlo simulations and the finite-size scaling used to analyze the Monte Carlo data. Section IV contains the details of the transfer-matrix calculations and the finite-size scaling relations used to analyze the transfer-matrix data. Section V contains our Monte Carlo and transfer-matrix data, the analysis of this data, and our results for the phase diagrams and critical exponents. Section VI presents a discussion of our results and conclusions.

II. MODEL AND GROUND STATES

We have studied the lattice-gas model with locally anisotropic next-nearest-neighbor interactions introduced by Wille *et al.*[18] to describe ordering of oxygen atoms in the Cu-O basal planes of $YBa_2Cu_3O_{6+x}$. These planes consist of a square lattice of copper atoms with lattice constant a and a basis of two oxygen sites at $(a/2,0)$ and $(0,a/2)$. The Hamiltonian is

$$\mathcal{H}-\mu N_a = -\Phi_{\rm NN}\sum_{\rm (NN)} c_i c_j - \Phi_{\rm Cu}\sum_{\rm (NNN_{Cu})} c_i c_j - \Phi_V \sum_{\rm (NNN_V)} c_i c_j - \mu\sum_i c_i . \quad (1)$$

Here the c_i are the site-occupation variables for the O atoms; $c_i = 1$ if site i is occupied, and $c_i = 0$ if site i is empty. $\Phi_{\rm NN}$ is the nearest-neighbor (NN) interaction energy, and $\Phi_{\rm Cu}$ and Φ_V are the next-nearest-neighbor (NNN) interaction energies, with and without a Cu atom between the O sites, respectively. The sums run over all the indicated pairs of sites. The oxygen chemical potential is μ, and N_a is the total number of O atoms. The basal-plane lattice and the interactions in the Hamiltonian are shown in Fig. 1. The oxygen concentration in the basal planes, Θ, is twice the factor x in the stoichiometric formula $YBa_2Cu_3O_{6+x}$,

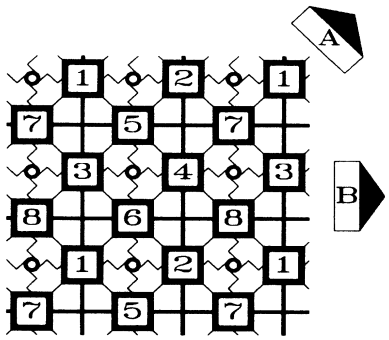

FIG. 1. The lattice in the basal CuO planes, and the interactions in the lattice-gas Hamiltonian, Eq. (1), are illustrated. The open circles represent Cu atoms, and the numbered squares represent the O sites. The nearest-neighbor interactions ($\Phi_{\rm NN}$) are shown as thin diagonal lines, the next-nearest-neighbor interactions through a copper ($\Phi_{\rm Cu}$) and through a vacancy (Φ_V) are shown respectively as zig-zag lines and thick solid lines. The numbering of the eight sublattices that define the Monte Carlo order parameter are shown. The arrows marked A and B show directions for the transfer matrix. Direction A would have, for example, the layer of sites along the diagonal numbered 7-3-6-2-7- interacting with the layer 1-5-4-8-1-. Direction B would have, for example, the layer of sites along a vertical zig-zag numbered 1-7-3-8-1- interacting with the layer 2-5-4-6-2-. This lattice is rotated by 45° with respect to those shown in Fig. 2(a).

$$\Theta = \frac{N_a}{N} = \frac{1}{N}\sum_i c_i = \frac{x}{2}, \quad (2)$$

where N is the total number of O sites.

As discussed in Sec. I, the experimentally observed phases are the tetragonal phase with $\Theta \simeq 0$, the "double-cell" orthorhombic phase with $\Theta \simeq \frac{1}{4}$, and the orthorhombic phase with $\Theta \simeq \frac{1}{2}$. For brevity we shall refer to these phases as tetra-0, ortho-$\frac{1}{4}$, and ortho-$\frac{1}{2}$, respectively. The corresponding orthorhombic ground states are depicted in Fig. 2(a). Both of these states are characterized by parallel chains of O atoms connected by Cu atoms. These ordered states can be described by decomposing the original lattice of O sites into eight interpenetrating sublattices, as shown in Fig. 1. The ordered state ortho-$\frac{1}{2}$ corresponds to four filled sublattices and four empty ones. This "antiferromagnetic" state is twofold degenerate. The ordered state ortho-$\frac{1}{4}$ corresponds to two filled sublattices and six empty ones. There are four equivalent pairs of sublattices that can be filled, making this state fourfold degenerate. This decomposition is used in defining Monte Carlo order parameters, as described in Sec. III A below.

The Hamiltonian and the interaction constants, Eq. (1), must be chosen to reproduce the observed phases.

This was achieved through a Landau-Lifshitz group-theoretical analysis[31-34] for this model, which identifies those ordered states compatible with the symmetry of the model that can be reached from a disordered state by a second-order (continuous) phase transition. Our analysis is similar to that of de Fontaine *et al.*;[12] however, we exactly obtain the ground-state diagram in terms of the oxygen chemical potential μ. Depending on the values of the interaction constants, a number of different ground-state diagrams may result. The one that corresponds to the experimentally observed phases is shown in Fig. 2(b). It acts as a guide to the low-temperature behavior for the Monte Carlo and transfer-matrix calculations. This ground-state diagram is realized only for repulsive NN interactions, $\Phi_{NN} < 0$, with NNN interactions in the ranges $\Phi_{Cu} > 0$ (attractive), and $-1 < \Phi_V/|\Phi_{NN}| < 0$ (weakly repulsive). In the following we shall use dimensionless units such that $\Phi_{NN} = -1$. The calculation also shows that an infinite number of states with parallel oxygen chains and $\Theta < \frac{1}{4}$ are degenerate with the ortho-$\frac{1}{4}$ and tetra-0 states exactly at their disorder-order transition. Consistent with these results we have chosen the NNN interactions $\Phi_{Cu} = 0.5$ and $\Phi_V = -0.5$, in agreement with Wille *et al.*[18] Preliminary finite-temperature transfer-matrix data support the expectation that, within the range of interactions consistent with the observed phases, the qualitative features of the phase diagrams do not depend on the particular values of the constants. These results and the ground-state diagrams for different values of the interaction constants will be given in a forthcoming paper.[35]

A Ginzburg-Landau effective free-energy calculation[31,32] indicates that, if continuous, the disorder-order transition tetra-0 to ortho-$\frac{1}{2}$ and the order-order transition ortho-$\frac{1}{4}$ to ortho-$\frac{1}{2}$ both should belong to the Ising universality class.[28] A similar calculation indicates that the disorder-order transition tetra-0 to ortho-$\frac{1}{4}$ most likely belongs to the universality class of the XY model with cubic anisotropy.[28] The phase diagram is similar to that of the Ashkin-Teller model.[28,36] These results are supported by our scaling analyses, presented in Sec. V.

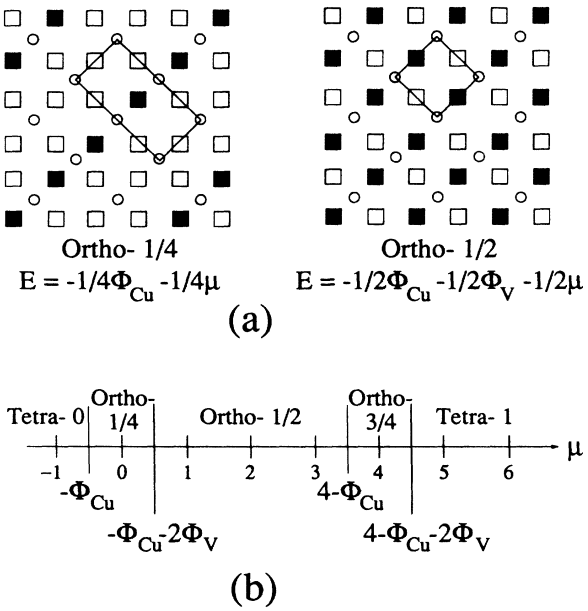

FIG. 2. (a) The ground-state configurations in the basal Cu-O planes, corresponding to the experimentally observed phases ortho-$\frac{1}{4}$ and ortho-$\frac{1}{2}$ are shown. Cu atoms are denoted by small open circles, O atoms by solid squares, and empty O sites by open squares. For each state the corresponding unit cell on the Cu lattice is drawn, and the energy per O site is given. Notice the characteristic chains of alternating O and Cu atoms. (b) Ground-state diagram showing the transition values of the chemical potential, μ, for the ground states when $\Phi_{Cu} > 0$ and $-1 < \Phi_V < 0$ (with $\Phi_{NN} = -1$). The transition values of μ are given as functions of Φ_{Cu} and Φ_V. The ortho-$\frac{3}{4}$ state is similar to the ortho-$\frac{1}{4}$ state except that the O vacancies and atoms are interchanged. The tetra-1 state corresponds to the completely filled lattice, just as the tetra-0 state corresponds to the completely empty lattice. The tetra-1 and ortho-$\frac{3}{4}$ states are not experimentally observed in $YBa_2Cu_3O_{6+x}$.

III. MONTE CARLO CALCULATIONS

A. Simulations

In our Monte Carlo calculations we have made use of standard importance sampling methods.[37-41] Most of the calculations were performed using single-spin-flip Glauber dynamics, where the oxygen concentration Θ is a function of T and μ. We have also performed some Monte Carlo calculations using Kawasaki dynamics, i.e., with Θ kept constant during the simulation. This was done by only allowing the oxygen atoms to jump to vacant nearest- and next-nearest-neighbor sites on the lattice, while keeping their total number fixed. We have studied lattices with periodic boundary conditions for $4 \leq L \leq 128$. L is defined along the unit vectors of the Cu unit cell and measured in units of its lattice constant a, which is the next-nearest neighbor distance between oxygen sites. Thus, the total number of oxygen sites is $N = 2L^2$.

The parallel chains of O atoms, discussed in Sec. II, are prominent features of the observed configurations. Even in the disordered state, rather long fragments of such chains are seen. (At low temperatures, $k_BT \leq 0.05$, these chains may span the whole lattice, even for the largest systems we have studied, $L = 128$.) Because of these long chain fragments, long runs are needed to get good statistics in the critical regions. Data were obtained with 5×10^4 to 5×10^5 Monte Carlo steps per oxygen site (MCSS), using every tenth generated configuration for calculating averages. For the transition from the disordered phase tetra-0 to the ordered phase ortho-$\frac{1}{4}$, we have also done some calculations using the block-distribution (cumulant) method[42,43] [see Eq. (9)] for analysis of the critical point. For this analysis we used much longer runs:

2×10^6 MCSS for $L \leq 32$.

In the Monte Carlo simulations the internal energy, U, the specific heat, C, the oxygen concentration, Θ, and the sublattice concentrations, Θ_α, (all quantities normalized per O site) are given by

$$U = \frac{1}{N}\langle \mathcal{H} \rangle, \qquad C = \frac{N}{(k_B T)^2}(\langle U^2 \rangle - \langle U \rangle^2), \tag{3}$$

$$\Theta = \frac{1}{N}\Big\langle \sum_i c_i \Big\rangle, \tag{4}$$

$$\Theta_\alpha = \frac{8}{N}\Big\langle \sum_{i \in \alpha} c_i \Big\rangle, \qquad \alpha = 1, 2, \ldots, 8. \tag{5}$$

The sublattices α are indicated in Fig. 1.

In terms of the sublattice concentrations Θ_α we have defined the two order parameters

$$\Theta_{1/2} = \tfrac{1}{4}\left|\Theta_1 + \Theta_2 + \Theta_3 + \Theta_4 - \Theta_5 - \Theta_6 - \Theta_7 - \Theta_8\right| \tag{6}$$

and

$$\Theta_{1/4} = \tfrac{1}{2}\left|(\Theta_1 + \Theta_2) - (\Theta_3 + \Theta_4) + (\Theta_5 + \Theta_6) - (\Theta_7 + \Theta_8)\right|, \tag{7}$$

where the subscript $\frac{1}{2}$ stands for the ortho-$\frac{1}{2}$ phase, and the subscript 1/4 for the ortho-$\frac{1}{4}$ phase. The order parameter $\Theta_{1/2}$ is unity in the ortho-$\frac{1}{2}$ phase, zero in the disordered phase tetra-0, and 0.5 in the ortho-$\frac{1}{4}$ phase. On the other hand, $\Theta_{1/4}$ is unity in ortho-$\frac{1}{4}$ and zero in both tetra-0 and ortho-$\frac{1}{2}$. In this sense, $\Theta_{1/4}$ is a "good" order parameter for the ortho-$\frac{1}{4}$ phase. The susceptibility conjugate to $\Theta_{1/4}$ is

$$\chi_{1/4} = \frac{N}{k_B T}\left(\langle \tilde{\Theta}_{1/4}^2 \rangle - \langle \tilde{\Theta}_{1/4} \rangle^2\right), \tag{8}$$

where $\tilde{\Theta}_{1/4}$ is given by Eq. (7) without the absolute values. An analogous definition for $\chi_{1/2}$ is also used. Following Binder,[42,43] we have also used the cumulants

$$U_L = 1 - \frac{\langle \Theta^4 \rangle_L}{3\langle \Theta^2 \rangle_L^2} \tag{9}$$

for the different order parameters to obtain the critical exponents ν and β [Eq. (14) and (15)]. U_L has previously been used with good results for a similar model.[44]

B. Finite-size scaling relations

The behavior of finite systems near the critical temperature T_c of the corresponding infinite system can be analyzed by finite-size scaling.[37–39,45–47] If the infinite system has the critical exponents, as usually defined, the behavior of the finite system is expressed in terms of a scaled temperature $x = tL^{1/\nu}$ where $t = |1 - T/T_c|$. Near T_c one can write finite-size scaling relations for sufficiently large L,

$$\Theta = L^{-\beta/\nu} f(x) \sim t^\beta \qquad \text{as } L \to \infty, \quad t \neq 0, \tag{10}$$

$$\chi T = L^{\gamma/\nu} g(x) \begin{cases} \sim L^{\gamma/\nu} & \text{for } t = 0, \\ \sim t^{-\gamma} & \text{as } L \to \infty, \quad t \neq 0, \end{cases} \tag{11}$$

$$C - C_0 = L^{\alpha/\nu} h(x) \begin{cases} \sim L^{\alpha/\nu} & \text{for } t = 0, \\ \sim t^{-\alpha} & \text{as } L \to \infty, \quad t \neq 0, \end{cases} \tag{12}$$

where C_0 is the nondivergent contribution to the specific heat. The critical behavior can also be determined by comparing cumulants and moments for lattices of size L with lattices of size $L' = bL$. At T_c, where $U = U^*$, one has[42,43]

$$U_L = U_{bL} = U^*, \tag{13}$$

$$\nu^{-1} = \frac{\ln(\partial U_{bL}/\partial U_L)_{U^*}}{\ln b}, \tag{14}$$

and

$$\frac{2\beta}{\nu} = -\ln\left(\langle \Theta^2 \rangle_{bL} / \langle \Theta^2 \rangle_L\right) / \ln b. \tag{15}$$

Because of correction terms to finite-size scaling, it is necessary to extrapolate the results to the limit $(\ln b)^{-1} \to 0$.

IV. TRANSFER-MATRIX CALCULATIONS

A. Transfer-matrix formulation

We have performed transfer-matrix finite-size scaling calculations to complement the Monte Carlo simulations, and especially to determine the order of the transitions at low temperatures. In the usual fashion, strip-shaped systems of infinite length and finite width M were partitioned into transverse layers. The results presented here were obtained with the partitioning, labeled A in Fig. 1, which leaves all three ground states invariant under a 90° rotation of the lattice. (For partitioning, B oxygen chains parallel and perpendicular to the strip direction have different energies, leading to large finite-size effects.)

The full transfer matrix $\mathbf{T}$, which is nonsymmetric, was block diagonalized utilizing the invariance of the Hamiltonian under two-step translations in the transverse direction. The symmetric block $\mathbf{T^S}$ and the antisymmetric block $\mathbf{T^A}$, the only two blocks whose symmetries correspond to the ordered phases ortho-$\frac{1}{2}$ and ortho-$\frac{1}{4}$, were diagonalized with the NAG library subroutines F02AFF and F02AGF. Four of the eigenvalues are of particular interest. The largest eigenvalue of $\mathbf{T^S}$, and of the full transfer matrix itself, is λ_1^S. By virtue of the Perron-Frobenius theorem it is positive and nondegenerate. The other three are λ_2^S and λ_3^S, second and third largest eigenvalues of $\mathbf{T^S}$, respectively, and λ_1^A, the largest eigenvalue

of $\mathbf{T}^{\mathbf{A}}$. The two eigenvalues λ_2^S and λ_1^A alternate as the second largest eigenvalue of $\mathbf{T}$. These four eigenvalues define the following three length scales.

$$\xi_1^S = \left(\ln\left|\frac{\lambda_1^S}{\lambda_2^S}\right|\right)^{-1} \tag{16}$$

is the largest length corresponding to $\mathbf{T}^{\mathbf{S}}$. It diverges exponentially with M in both the ortho-$\frac{1}{4}$ and ortho-$\frac{1}{2}$ ordered phases.

$$\xi_2^S = \left(\ln\left|\frac{\lambda_1^S}{\lambda_3^S}\right|\right)^{-1} \tag{17}$$

is the second largest length corresponding to $\mathbf{T}^{\mathbf{S}}$. It remains small and independent of M in both the ordered phases, but peaks near the transitions involving the ordered ortho-$\frac{1}{4}$ phase.

$$\xi_1^A = \left(\ln\left|\frac{\lambda_1^S}{\lambda_1^A}\right|\right)^{-1} \tag{18}$$

is the largest length corresponding to $\mathbf{T}^{\mathbf{A}}$. It uniquely characterizes the ortho-$\frac{1}{4}$ phase, where it diverges exponentially with M, whereas it remains small and independent of M in the ortho-$\frac{1}{2}$ ordered phase, as well as in the disordered tetra-0 phase. At the tetra-0 to ortho-$\frac{1}{2}$ transition ξ_1^S is the overall dominant length scale. At the tetra-0 to ortho-$\frac{1}{4}$ transition ξ_1^A and ξ_1^S are of the same order of magnitude, with ξ_1^A generally dominant. (However, at temperatures below k_BT=0.1, ξ_1^S becomes dominant for M=12.)

For the largest system size, $M = 16$, an entire block of the transfer matrix could not be stored in the available computers, so an alternative numerical method was implemented. By using the structure of the full transfer matrix as given by generalized direct matrix products,[48,49] it was efficiently constructed when needed using scatter and gather operations on the **Cyber 205** and **ETA-10** computers. The transfer matrix was repeatedly multiplied by a random starting vector to obtain the largest eigenvalue and the associated left and right eigenvectors. The next largest eigenvalue was constructed in a similar fashion.[50] This procedure gave the largest length scale and Θ, and their derivatives were taken numerically. (This method does not directly provide information about the symmetry of the eigenvectors, but the results for $M = 8$ and 12 compared very well with those obtained with the method described above.)

B. Finite-size scaling relations

In the finite-size scaling theory for critical phenomena a second-order phase transition is signaled by the linear divergence with strip width M of the appropriate dominant length scale, $\xi(M)$. A finite-size estimate for the critical values of the nonordering fields is given by the Nightingale criterion,[51,52]

$$\frac{\xi(M)}{M} = \frac{\xi(M')}{M'}. \tag{19}$$

For each of the three different transition lines in the present model ξ represents the appropriate characteristic length scale, as discussed in Sec. IV A above.

The thermal eigenvalue, $y_T = \nu^{-1}$, is related to the asymptotic scaling at the critical point of the gradient $\nabla_{\mathbf{K}}\xi(M)$ of the dominant correlation length with respect to the nonordering fields, $\mathbf{K} = (\beta, \beta\mu)$, where $\beta = 1/k_BT$, as

$$y_T + 1 \simeq \left(\ln\frac{\mathbf{v}\cdot\nabla_{\mathbf{K}}\xi(M)}{\mathbf{v}\cdot\nabla_{\mathbf{K}}\xi(M')}\right)\left(\ln\frac{M}{M'}\right)^{-1}. \tag{20}$$

The notation $\mathbf{v}\cdot$ denotes the scalar product with a unit vector $\mathbf{v}$ in $\mathbf{K}$ space. In the asymptotic limit the gradients for M and M' become parallel, so that the estimate obtained from Eq. (20) is the same for all $\mathbf{v}$ that are not strictly orthogonal to the gradient. (In other words, y_T is invariant under independent rescalings of the fields.) However, for finite systems the estimate depends on the direction of $\mathbf{v}$.[53] We have chosen $\mathbf{v}$ to minimize this dependence. The resulting vectors $\mathbf{v}$ are, in fact, finite-size estimates of the relevant scaling field at each point on the transition line. (This estimation method differs from that described by Barber,[53] but for these relatively small systems we find our estimate more robust.) To avoid numerical differentiation for $M \leq 12$, we have related the field derivatives of ξ to matrix elements of certain operators, as described in the Appendix, Eq. (28). For $M = 16$ we used numerical differentiation, since the blocks of the transfer matrix were too large to store in the available computers.

First-order transitions to the ortho-$\frac{1}{4}$ phase have been sought by two different scaling methods. First, the maximum of the second largest symmetric length scale, ξ_2^S, which peaks near the transition, was monitored for linear divergence with M to detect a possible tricritical point. This method is quite accurate for systems with a relatively simple eigenvalue spectrum.[54–56] However, in complicated systems, such as the present one, degeneracies and large finite-size effects may obscure the choice of the proper secondary length scale.

Since a first-order transition corresponds to a discontinuity in Θ, it is signaled by an exponential divergence with M in the maximum value, $\chi_\Theta^{\max}$, of the nonordering susceptibility. Finite-size scaling of $\chi_\Theta^{\max}$ therefore constitutes an alternative method to identify a first-order transition. Since the nonordering susceptibility contains contributions from a large number of microscopic lengths in addition to the proper secondary length scale, this method is less sensitive than the direct finite-size scaling of the secondary length. However, it is more robust in the sense that it does not require unambiguous identification of the appropriate length scale. For systems to which both methods have been applied, they yield consistent

results. A detailed discussion and comparison is given by Rikvold,[57,58] where the following scaling relation is obtained:

$$\frac{\chi_\Theta^{\max}(M)}{M} = \frac{\chi_\Theta^{\rm reg}}{M} + \begin{cases} A_1 \exp\left(\frac{M}{k_B T}\sigma(T,\mu)\right), & T<T_m \\ A_m M^{1-\tilde{\eta}_m}, & T=T_m \\ A_2(M), & T>T_m \end{cases} \tag{21}$$

Here $\chi_\Theta^{\rm reg}$ is the regular part of χ_Θ, $\sigma(T,\mu)$ is a surface tension associated with phase coexistence below the multicritical temperature T_m, and $\tilde{\eta}_m = 2 - 2/\nu_m + d$ is the correlation-length exponent for a d-dimensional system, corresponding to an approach to the multicritical point *parallel* to the line of critical points. The factor A_2 may depend logarithmically on M, due to coupling to the specific heat. For non-Ising like systems its M dependence might be even stronger, although we see no signs of this for the present system. To avoid numerical differentiation for $M \leq 12$, we expand χ_Θ in matrix elements of the concentration operator Θ.[59] The explicit expression is shown in the Appendix, Eq. (29). For $M = 16$ the derivatives were taken numerically, as discussed above.

V. RESULTS

A. Phase diagrams

Our phase diagrams, obtained by finite-size scaling analysis of data from Monte Carlo and transfer-matrix calculations, are shown in Fig. 3 and Fig. 4: projections onto the Θ, T plane in Fig. 3 and onto the μ, T plane in Fig. 4. The Monte Carlo simulations were performed with both Glauber and Kawasaki dynamics on systems with L between 8 and 128. Transfer-matrix calculations were performed with strip widths $M/M' = 4/8$ and $8/12$, and two points with $12/16$. (Only data for $M/M' = 8/12$ and $12/16$ are shown in Fig. 3 and Fig. 4.) For comparison, Fig. 3 also includes results from a cluster-variation calculation.[18] Experimental data from Specht *et al.*[8] were used to establish an estimated temperature scale along the right-hand vertical axes. To emphasize the consistency of the experimental data and the model, two independent data points from McKinnon *et al.*[60] were also included, without any further parameter adjustment. The Monte Carlo and transfer-matrix results are in excellent agreement with each other, and with the experimental data. Three lines of second-order phase transitions, merging at a multicritical point, separate the disordered tetra-0 phase and the two ordered phases, ortho-$\frac{1}{4}$ and ortho-$\frac{1}{2}$.

Also shown in the phase diagrams are the locations of the non-scaling peaks in the Monte Carlo specific heat, which correspond to disorder lines in the model. The half-width at half maximum of the nonscaling specific heat peak is also shown in Fig. 3 and Fig. 4. The disorder line in the disordered phase is that observed by de Fontaine *et al.*,[61] but they did not show the locations of the disorder lines in the phase diagram. Indications of a disorder line have also been seen in thermodynamic experiments.[60] We have been able to determine that these disorder lines are due to the formation of long chains of O atoms, and have obtained excellent agreement between the Monte Carlo results for the disorder lines and a treatment combining the methods of mean-field and one-dimensional systems for this model.[62] This provides further evidence that the disorder lines are due to the formation of chains, and that these chains order on the critical curve.

Finite-size effects are quite small for both the transfer-matrix and Monte Carlo results in the μ, T plane, except near the multicritical point where the three transition lines meet. In the Θ, T diagram the finite-size effects are considerable at low temperatures. In the transfer-matrix results this is due to the very large nonordering susceptibility, χ_Θ. In the Monte Carlo calculations the large finite-size effects at low temperatures are due to the formation of oxygen chains that span the entire lattice, even for the largest systems studied, $L = 128$. At these low temperatures, once the chains are formed, there is only a very small probability that there will be sizable fluctuations from this state; i.e., the relaxation times are very long. At temperatures down to $k_B T \simeq 0.15$ the results from Kawasaki dynamics agree with the results from Glauber dynamics for the disorder-order transitions. However, with Kawasaki dynamics we are unable to obtain the order-order transition, due to the large finite-size effects and the long relaxation times. To search for first-order coexistence lines, we also performed runs at low temperatures using Kawasaki dynamics. However, once the system has arranged itself with chains going through the whole sample, the probability for a single oxygen atom to jump is very small, thus the system seems frozen in. With Glauber dynamics, we also find that the chains can span the whole sample at $k_B T \simeq 0.1$. However, the nonconservation of Θ in this dynamics allows larger fluctuations in the chain length. The long relaxation times at low temperatures could be misinterpreted as metastability associated with a first-order transition. (Bear in mind that for a finite system there is no phase transition, and therefore no real critical behavior.) Consequently, whenever the relaxation time is large, finite-size scaling of the Monte Carlo data[63] or use of the Monte Carlo renormalization group method[64] is required to unambiguously identify the order of the transition.

Qualitatively, the phase boundaries are consistent with those obtained by Wille *et al.*[18] and Kikuchi and Choi,[27] using the cluster-variation method (CVM). The differences between the CVM critical temperatures and our nonperturbative results are concentration dependent and range from 5% to 21% for the transition between the disordered tetra-0 and the ordered ortho-$\frac{1}{2}$ phases. Consequently, in order to adjust the interaction constants to compare with experimental values, one should use Monte Carlo or transfer-matrix data rather than CVM calculations.[24] The CVM results indicate that both the

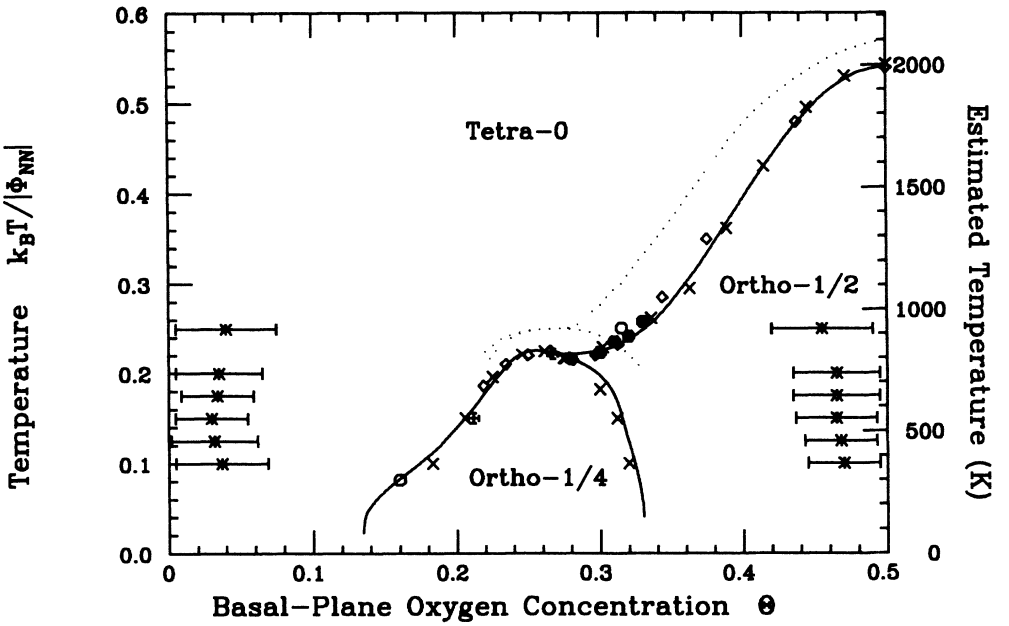

FIG. 3. The phase diagram in the Θ, T plane for interactions $\Phi_{NN} = -1$, $\Phi_{Cu} = 0.5$, and $\Phi_V = -0.5$ is shown. Three second-order lines, separating one disordered phase (tetra-0) and two ordered phases (ortho-$\frac{1}{4}$ and ortho-$\frac{1}{2}$), meet at a multicritical point. Also shown are experimental points due to Specht *et al.*[8] (solid circles), which are used to establish an estimated temperature scale along the right-hand vertical axis. Two experimental points from McKinnon *et al.* (Ref. 60) (open circles) were also included without further parameter adjustments. The *relative* error in the concentration determination for these latter points is of the order of ± 0.005, approximately equal to the symbol size (Ref. 60). Monte Carlo results are presented from finite-size scaling analysis of data, using both Glauber dynamics ($\times$) and Kawasaki dynamics ($\diamond$). The location ($*$) and half-width at half maximum for the nonscaling specific heat peak from Monte Carlo data is shown, giving the location of the disorder lines. The solid line is the transfer-matrix results from 8/12 scaling. Two data points for 12/16 scaling are also shown (roman crosses). The dotted lines are CVM results of Wille *et al.* (Ref. 18) for exactly the same interactions.

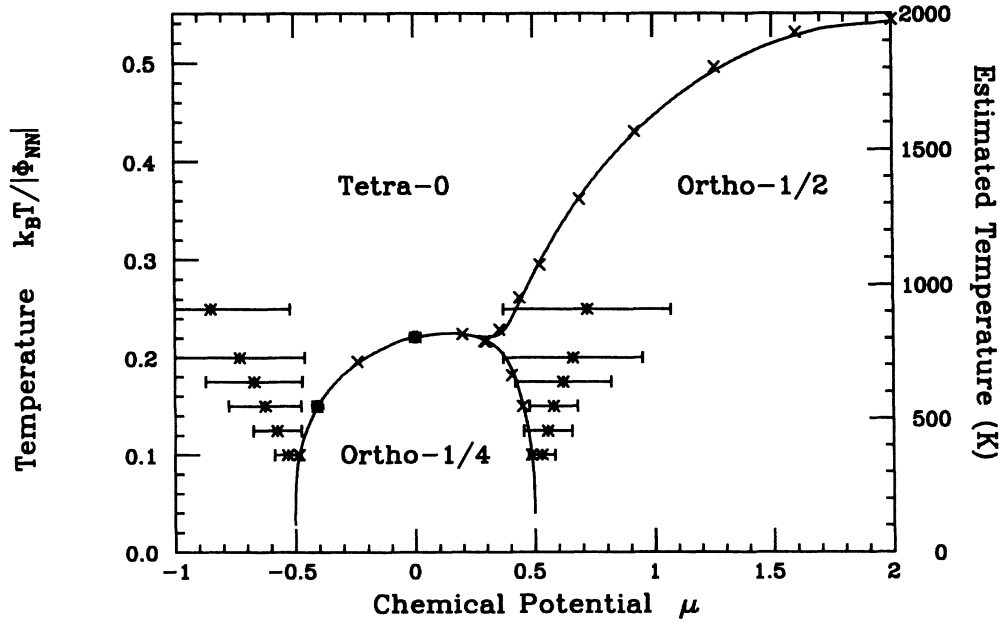

FIG. 4. The phase diagram in the μ, T plane, from Monte Carlo and transfer-matrix data, is shown. The system and symbols are the same as in Fig. 3. The results for different system sizes are hardly discernible on the scale of the figure.

tetra-0 to ortho-$\frac{1}{2}$ (Refs. 18 and 27) and ortho-$\frac{1}{4}$ to ortho-$\frac{1}{2}$ (Ref. 27) transitions are of second order, in agreement with our results (as discussed in Sec. V B). However, they predict that the transition from tetra-0 to ortho-$\frac{1}{4}$ is first order.[18,27] In contrast, our detailed scaling analysis of the Monte Carlo and transfer-matrix data indicates that all three transitions are of second order, at least down to $k_BT \simeq 0.025$ (corresponding to approximately 90 K on the estimated temperature scale). The quantity

$$\Delta\xi_2 = \frac{\xi_2^S(M+4)}{M+4} - \frac{\xi_2^S(M)}{M}, \tag{22}$$

which indicates the scaling behavior of the second largest symmetric length scale, is shown versus T in Fig. 5. For a first-order transition, $\Delta\xi_2$ is large and positive as $M \to \infty$, as discussed in Sec. IV B. We find that $\Delta\xi_2$ is negative for low T, and that the small positive values near the multicritical point at $k_BT \simeq 0.22$ decrease with increasing M. This is initial evidence that all the transitions in this system remain second order, even at low T. Further details of the scaling analysis and the orders of the transitions are presented below.

B. Transitions involving the ortho-$\frac{1}{2}$ phase

Transfer-matrix data for the critical exponent, $\nu = y_T^{-1}$, [Eq. (28)], obtained with strip widths $M/M' = 4/8$ and 8/12, are shown in Fig. 6 for the two transitions that involve the ortho-$\frac{1}{2}$ phase. At the disorder-order tetra-0 to ortho-$\frac{1}{2}$ transition ν rapidly approaches unity as the strip size increases. At the order-order ortho-$\frac{1}{4}$ to ortho-$\frac{1}{2}$ transition the finite-size effects are rather large, but there too, ν seems to approach unity as M increases. These results are consistent with the symmetry considerations in Sec. II, which indicate that, if continuous, both transitions should belong to the Ising universality class, for which $\nu = 1$. No changes in ν that might indicate multicriticality or first-order transitions are seen, except near the known multicritical point where the three transition lines meet. Our scaling estimate for the location of this point, based on the equality of $\xi_1^S(12)$ and $\xi_1^A(12)$, is $k_BT = 0.222 \pm 0.001$, $\mu = +0.23 \pm 0.02$. This point is believed to belong to the universality class of the four-state Potts model,[28,36] for which both the critical and tricritical values of ν are $\frac{2}{3}$.[65] The minimum value of the 8/12 scaling estimates for ν from ξ_1^S occurs near this multicritical point, and is $\nu_{\min} \simeq 0.740$. In view of the large finite-size effects, this result is not inconsistent with the expected value of $\frac{2}{3}$.

At the tetra-0 to ortho-$\frac{1}{2}$ transition the Monte Carlo data give good finite-size scaling with Ising critical exponents for the order parameter $\Theta_{1/2}$ and susceptibility $\chi_{1/2}$. To illustrate this, in Fig. 7 we show the scaling relation for the maximum in $\chi_{1/2}$ for $\mu = 2.0$. We also performed finite-size scaling analyses similar to those shown

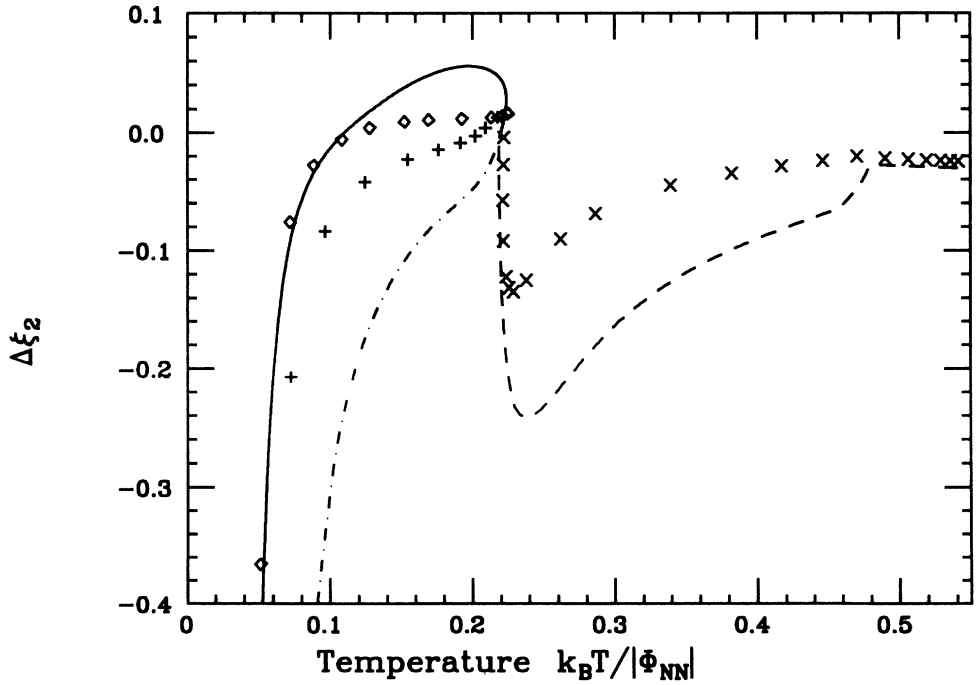

FIG. 5. The quantity $\Delta\xi_2$ defined in Eq. (22) is shown. As $M \to \infty$ negative values indicate a second-order transition, and positive values a first-order transition. Lines correspond to 4/8 scaling, data points to 8/12 scaling. The different transitions are tetra-0 to ortho-$\frac{1}{2}$ (dashed line and ×), ortho-$\frac{1}{4}$ to ortho-$\frac{1}{2}$ (dot-dashed line and +), and tetra-0 to ortho-$\frac{1}{4}$ (solid line and ◇).

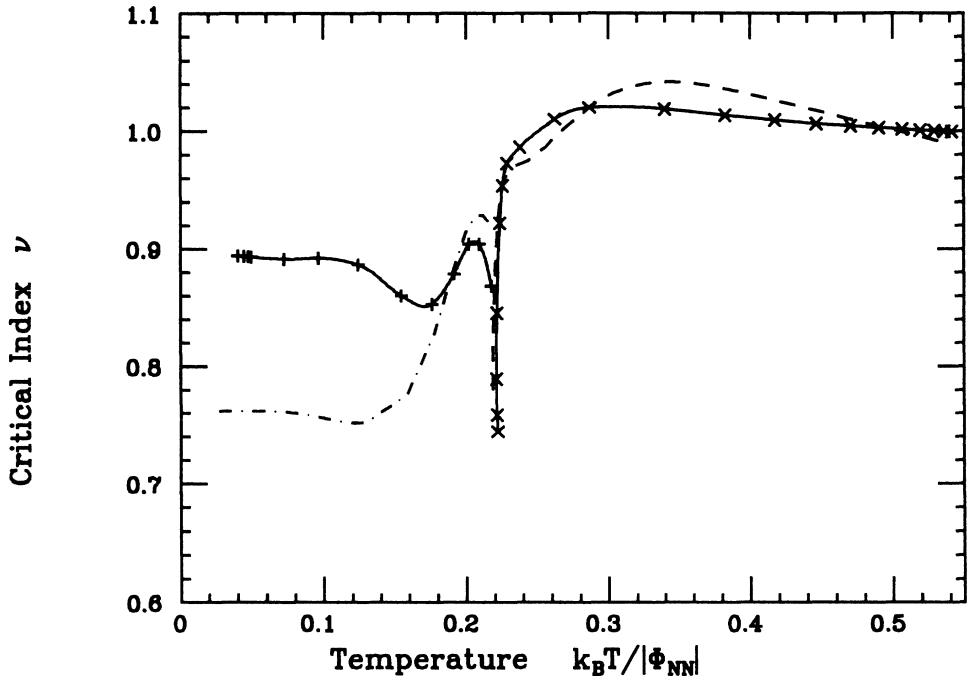

FIG. 6. The critical index ν for the tetra-0 to ortho-$\frac{1}{2}$ and ortho-$\frac{1}{4}$ to ortho-$\frac{1}{2}$ transitions, as obtained from 4/8 and 8/12 scaling of the transfer-matrix results. The dashed and dot-dashed lines correspond to 4/8 scaling at the tetra-0 to ortho-$\frac{1}{2}$ and ortho-$\frac{1}{4}$ to ortho-$\frac{1}{2}$ transitions, respectively. For the 8/12 scaling $\times$ and $+$ correspond to the tetra-0 to ortho-$\frac{1}{2}$ and ortho-$\frac{1}{4}$ to ortho-$\frac{1}{2}$ transitions, respectively. The solid lines through the 8/12 data points are guides for the eye.

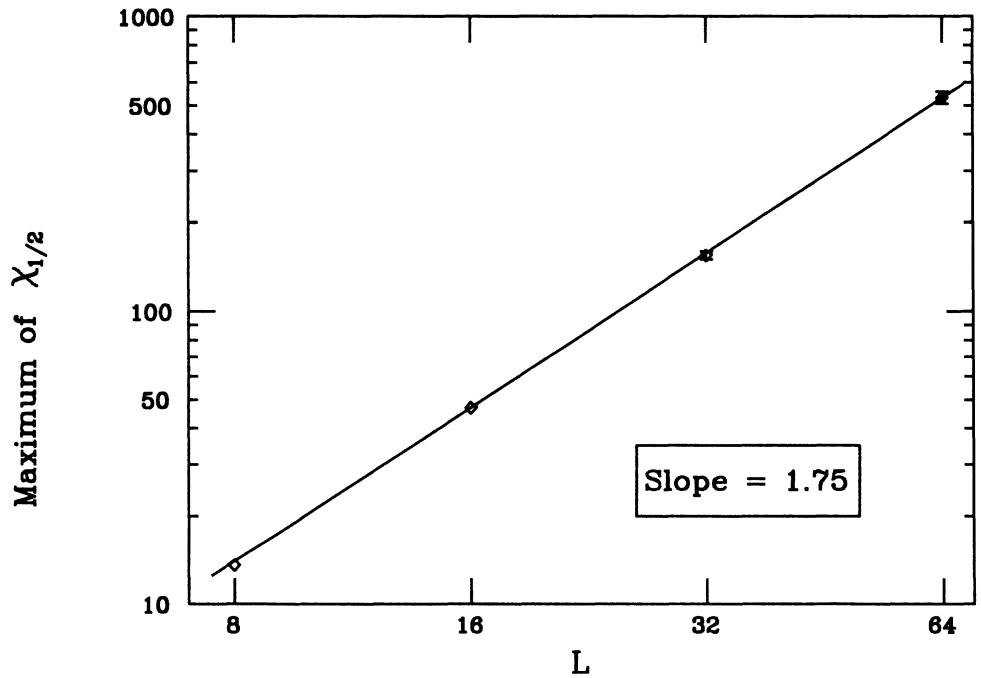

FIG. 7. The finite-size scaling of Monte Carlo data for the maximum of the susceptibility, $\chi_{1/2}^{\max}$ [Eq. (11)], at the highest temperature on the tetra-0 to ortho-$\frac{1}{2}$ transition line is shown. The transition, which belongs to the Ising universality class, occurs at $\mu_c = 2.000$, $T_c = 0.544$. The straight line has a slope of 1.75, which is the value of γ/ν for the 2d Ising model, as well as for all other models that obey Suzuki weak universality.

in Fig. 12 using $d = 2$ Ising exponents, and obtained good scaling. Similar scaling relations were obtained for the scaling of the Monte Carlo data for the other points along this transition line. Thus both the Monte Carlo and the transfer-matrix results for the critical exponents show that this transition belongs to the Ising universality class.

At the order-order transition, ortho-$\frac{1}{4}$ to ortho-$\frac{1}{2}$, the Monte Carlo data could again be fit to the scaling forms given by Eqs. (10)—(12) with Ising exponents. In the Monte Carlo runs at $k_BT = 0.15$, μ was varied at fixed temperature, so in the scaling expressions we have used the scaled chemical potential, $y = |1 - \mu/\mu_c|L^{1/\nu}$, instead of the scaled temperature, x. We found $\mu_c = 0.452 \pm 0.001$. (For other temperatures, the transition was approached along a direction that was "perpendicular" to the phase boundary determined from Monte Carlo simulations.) Fig. 8 shows an example of this scaling for $\chi_{1/4}$. Two difficulties can be seen in Fig. 8. The first is that the scaling function reaches its asymptotic value only for large values of y, which means that large systems must be simulated to reach the asymptotic region. The other difficulty is that near the critical point (small y) there are noticeable statistical fluctuations due to the fact that the chains have only very small fluctuations so the Monte Carlo dynamics is extremely slow. In spite of these difficulties, the Monte Carlo data illustrate that the transition at temperatures down to $k_BT = 0.15$ is second order and belongs to the Ising universality class. This is consistent with the transfer-matrix results (Figs. 5 and 6) for this transition.

We attempted to identify possible first-order behavior at low temperatures by observing hysteresis. We started from the two different ground states, corresponding to the ortho-$\frac{1}{4}$ and ortho-$\frac{1}{2}$ phases, and scanned μ at fixed temperature. With 2×10^3 MCSS we found large hysteresis for $k_BT \leq 0.05$. However, at these low temperatures the oxygen chains span the entire lattice, even for $L = 128$. Also, the hysteresis becomes less pronounced as the number of Monte Carlo steps is increased. These observations indicate that the apparent hysteresis most likely is due to large finite-size effects and strong critical slowing down at a second-order transition, rather than to true metastability associated with a first-order transition. At lower temperatures the relaxation is extremely slow, and we are unable to explore the phase transition in a satisfactory manner with our Monte Carlo algorithms.

The transfer-matrix programs used in this study remain effective down to lower temperatures than the Monte Carlo algorithm. In a further attempt at locating a possible low-temperature tricritical point below which the order-order transition might become first-order, we performed a transfer-matrix study of the scaling behavior of the maximum of the nonordering susceptibility, $\chi_\Theta^{\max}$, as discussed in Sec. IV B above. The results for strip widths $M = 4$, 8, and 12 at temperatures down to $k_BT = 0.025$ are displayed in Fig. 9. No indication of the characteristic exponential growth with M that signals a first-order transition [Eq. (21)] is seen. It cannot be entirely ruled out that this is due to a very large regular part, χ_Θ^{reg}, but in conjunction with the transfer-matrix and Monte Carlo evidence cited above, it indicates

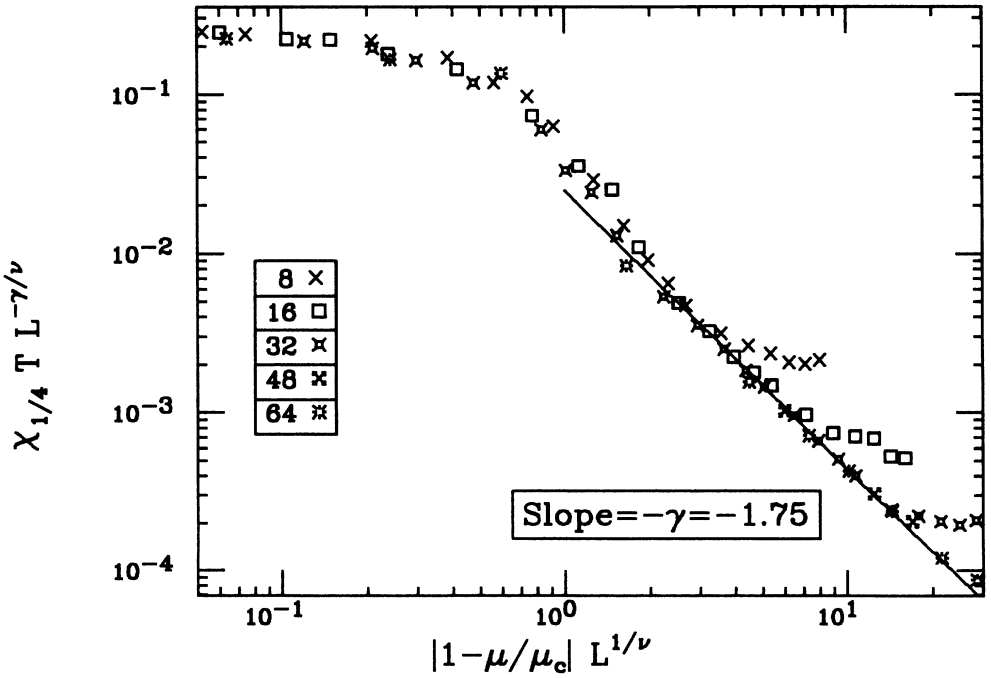

FIG. 8. Finite-size scaling of the Monte Carlo data for $\chi_{1/4}$ [Eq. (11)] at the ortho-$\frac{1}{4}$ to ortho-$\frac{1}{2}$ transition line is shown. The transition, which belongs to the Ising universality class, $\nu = 1$, occurs at $\mu_c = 0.4517$, $k_BT_c = 0.150$. The straight line has a slope of -1.75, which is the value of $-\gamma$ for the 2D Ising model. The nonscaling data tails provide an estimate for the size of the asymptotic critical region.

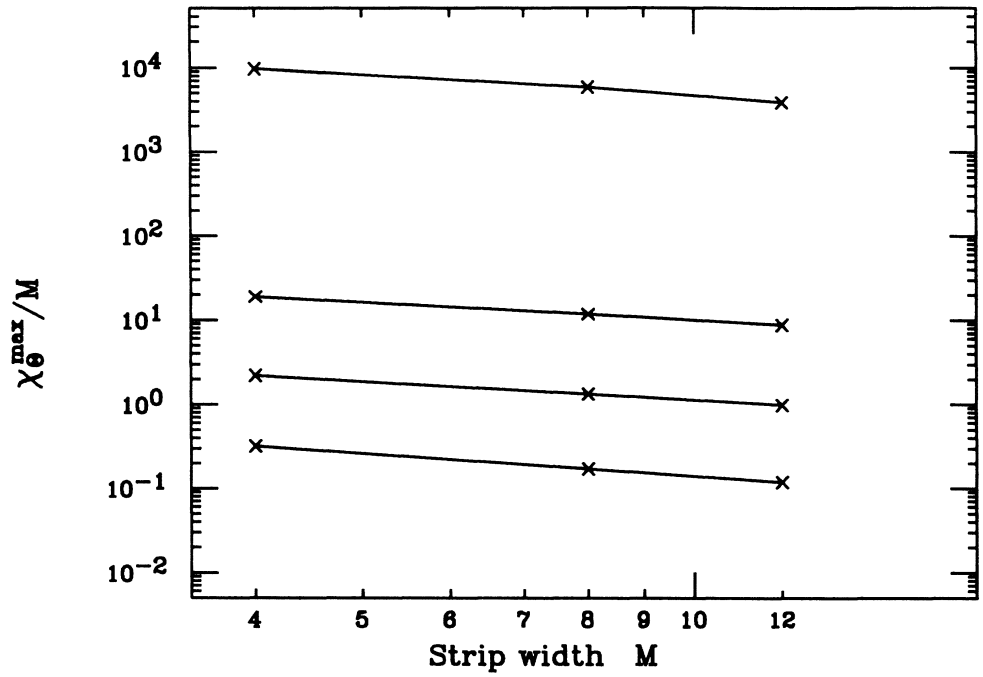

FIG. 9. Scaling plots for the maximum of the nonordering susceptibility, $\chi_\Theta^{\max}$, at the ortho-$\frac{1}{4}$ to ortho-$\frac{1}{2}$ transition, as obtained from transfer-matrix data are shown. The temperatures are (from below to above in the figure) $k_BT = 0.1625$, 0.0875, 0.055, and 0.025. No indication of the exponential growth with M that would signal a first-order transition is seen, even at the lowest of these temperatures.

that this transition remains second order at least down to $k_BT \simeq 0.025$. This conclusion is also consistent with the recent CVM results of Kikuchi and Choi.[27]

C. The disorder to ortho-$\frac{1}{4}$ transition

To determine the order and universality class of the disorder-order tetra-0 to ortho-$\frac{1}{4}$ transition we have performed a detailed Monte Carlo and transfer-matrix finite-size scaling analysis. This analysis confirms the initial hypothesis, stated in Sec. IV A and based on the behavior of the quantity $\Delta\xi_2$, that this transition, too, remains second order, at least down to $k_BT = 0.025$.

Our Monte Carlo study for this transition was concentrated at $k_BT = 0.15$, since this was the lowest temperature at which reasonable Monte Carlo data could be obtained with our algorithm. At lower temperatures prohibitively long runs are needed to get good statistics in the Monte Carlo sampling. This temperature is also low enough so cross-over effects due to the multicritical point should be negligible.

At a critical point the maximum of the singular part of the specific heat, $C_{\max} - C_0$, scales asymptotically as $L^{\alpha/\nu}$ [Eq. (12) with $x = 0$]. The best fit was obtained for $\alpha/\nu = 0.82 \pm 0.03$, where the value of C_0 that gives the best fit depends on the value of α/ν. Together with the hyperscaling relation, $d\nu = 2 - \alpha$, this yields $\nu = 0.71 \pm 0.02$ and $\alpha = 0.59 \pm 0.02$. Good fits could also be obtained by neglecting the $L = 8$ data (this size may be so small that $C_{\max}$ falls outside the asymptotic scaling region), which gives comparable values of α/ν, but different nondivergent parts of the specific heat, C_0. One such plot is shown in Fig. 10(a), where the values of C_0, ν, and α from the full finite-size scaling presented below are used. At the critical point the maximum of the susceptibility, $\chi_{1/4}$, scales asymptotically as $L^{\gamma/\nu}$ [Eq. (11) with $x = 0$]. We obtain a best fit with $\gamma/\nu = 1.75 \pm 0.03$, which, combined with $\nu = 0.71 \pm 0.02$, yields $\gamma = 1.24 \pm 0.05$. Figure 10(b) shows that this model obeys, to within the uncertainties in the simulation, Suzuki weak universality[66] for which $\gamma/\nu = \frac{7}{4}$.

In order to obtain an independent estimate of ν we have also calculated the cumulant U_L, Eq. (9), for the order parameter $\Theta_{1/4}$. In Fig. 11(a) we show U_L versus U_8. The data are averages over two independent runs of 2×10^6 MCSS each for $L = 8$, 12, 16, and 32. The lines in Fig. 11(a) represent linear fits to the data close to the intersection where $U_8 = U_L$. The dependence of the critical exponents on the scale factor $b = L'/L$ between the two lattices being compared is shown in Figs. 11(b) and (c). As seen in Fig. 11(b), the uncertainties are too large to obtain a very accurate estimate of ν. We find $\nu = 0.70 \pm 0.05$, which is consistent with the above estimate of $\nu = 0.71 \pm 0.02$. To obtain $2\beta/\nu$ [from Eq. (15)] we also tried to use data for $L = 4$ [Fig. 11(c)]. However, the finite-size effects for $L = 4$ are too large to obtain

reasonable estimates. The estimates for $2\beta/\nu$ from $L = 8$ and $L = 12$ agree reasonably well, to within about 5%. The best extrapolations with $1/\ln b$ for $L = 8$ and $L = 12$ also approach the value $2\beta/\nu = \frac{1}{4}$ as L is increased. This value of $2\beta/\nu$ is expected from the scaling relation $2\beta + \gamma + \alpha = 2$, the hyperscaling relation $d\nu = 2 - \alpha$, and the value $\gamma/\nu = 1.75$ from Fig. 10(b). The crossing of U_L for different L yields the critical chemical potential $\mu_c = -0.4073 \pm 0.0002$, which is consistent with the best finite-size scaling plots, which we present below.

The best finite-size scaling plot for the specific heat in the ordered ortho-$\frac{1}{4}$ phase is shown in Fig. 12(a). In it

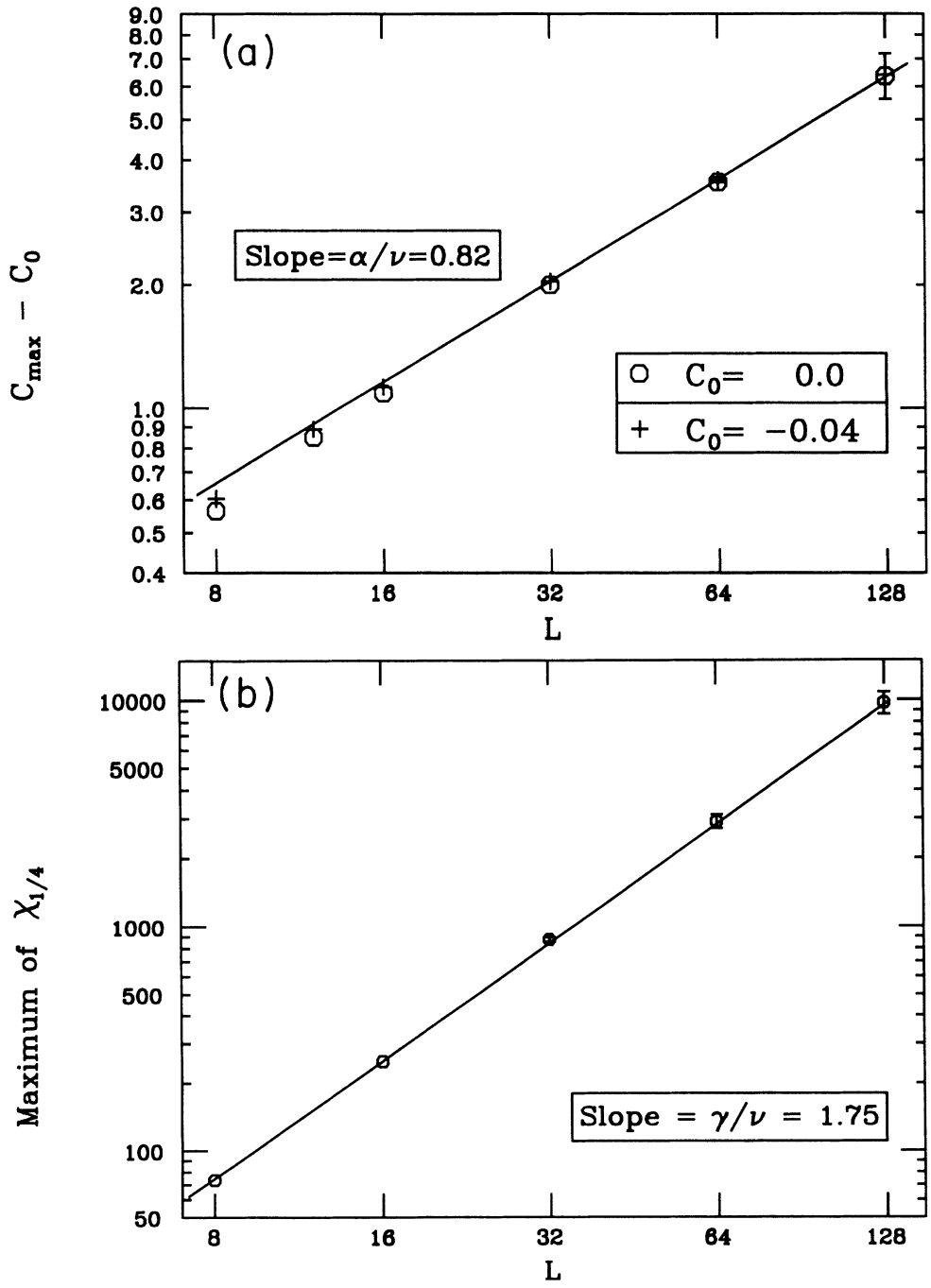

FIG. 10. Scaling plots of Monte Carlo data at the disorder to ortho-$\frac{1}{4}$ transition for $k_BT = 0.15$ are shown. (a) The maximum of the divergent part of the specific heat $C - C_0$ is shown. The value $C_0 = -0.04$ is the value obtained from the scaling plot of Fig. 12(a). The straight line has a slope of α/ν, with α and ν taken from the scaling plot of Fig. 12(a). (b) The maximum of the order-parameter susceptibility $\chi_{1/4}$ is shown. The straight line has a slope of 1.75, which gives γ/ν.

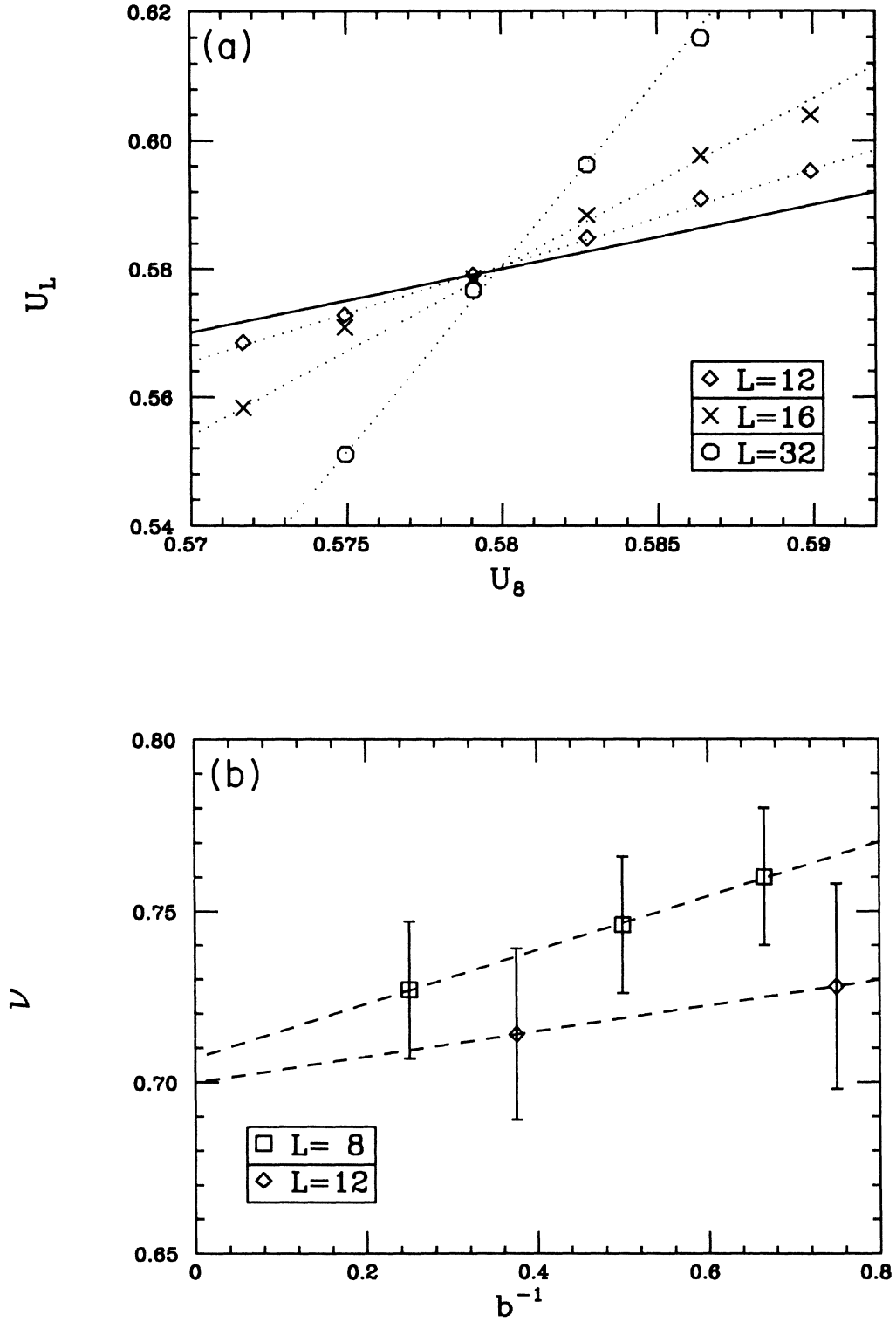

FIG. 11. We show data for the cumulant given in Eq. (9) for $\Theta_{1/4}$ at $k_BT = 0.15$. (a) Shows the cumulant U_L plotted vs U_8 at the disorder to ortho-$\frac{1}{4}$ transition, and the best linear fits for the data at the intersection point where $U_L = U_8$. (b) Shows the data from the linear fits in (a) to obtain ν from Eq. (14). The dashed lines show the best linear extrapolations to $b \to \infty$. (c) Shows the extrapolation of the linear fits to obtain $2\beta/\nu$ from Eq. (15). The data for $L = 4$ have noticeable finite-size effects. The lines are the best linear fits to the data for $L = 8$ and $L = 12$. The arrow shows the location of $2\beta/\nu = \frac{1}{4}$, which is obtained from assuming $\gamma/\nu = \frac{7}{4}$, the hyperscaling relation $d\nu = 2 - \alpha$, and the scaling relation $\alpha + 2\beta + \gamma = 2$.

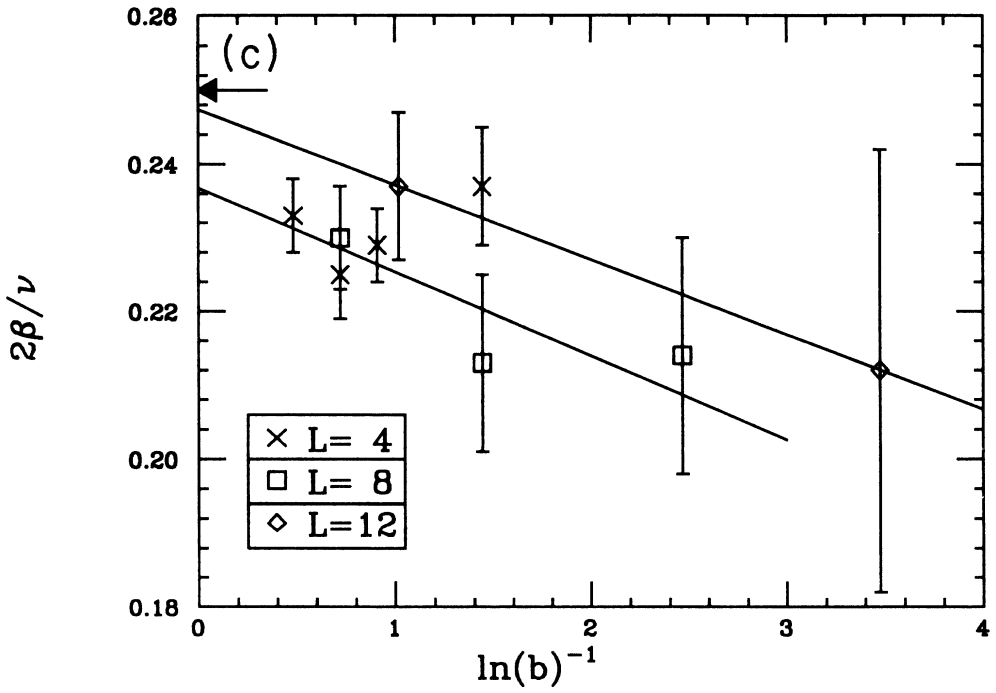

FIG. 11. (*Continued*).

we use $\mu_c = -0.4074$ at $k_BT_c = 0.15$, together with $C_0 = -0.04$ and the exponents $\alpha = 0.58$ and $\nu = 0.71$. Good finite-size scaling for $\chi_{1/4}$ in the ortho-$\frac{1}{4}$ phase is obtained for this value of μ_c with $\gamma = 1.2425$, so that $\gamma/\nu = \frac{7}{4}$. To obtain consistent values of μ_c and ν, we found we needed to use the scaling variable $y' = |1 - \mu_c/\mu|L^{1/\nu}$ for $\chi_{1/4}$, as is often the case for susceptibilities.[38] Figure 12 shows that the scaling functions reach their asymptotic region only for large values of y or y', which requires large lattice sizes. However, for large lattices, statistical errors due to critical slowing down give large errors, particularly close to μ_c. Nevertheless, reasonable scaling for C, $\Theta_{1/4}$ and $\chi_{1/4}$ in both the tetra-0 and the ortho-$\frac{1}{4}$ phases is obtained using the parameters in Fig. 12, together with $\beta = \nu/8$ so that $2\beta/\nu = \frac{1}{4}$.

All the finite-size scaling results are consistent and indicate a second-order transition in the universality class of the XY model with cubic anisotropy, which has variable exponents. This behavior is expected from a Ginzburg-Landau effective free-energy calculation.[28] Although this provides a strong indication of the universality class, it does not constitute an absolute proof. It is conceivable that one component of the Ginzburg-Landau order parameter may act as an effective field, driving another mode unstable, and thus effectively increase the dimension of the order parameter. If this happened, the model could be in the universality class of the four-state Potts model. Since the critical exponents found above are close to those of the four-state Potts model, $\nu = \frac{2}{3}$, $\alpha = \frac{2}{3}$, $\beta = \frac{1}{12}$, and $\gamma = \frac{7}{6}$, we have also performed finite-size scaling for C, $\Theta_{1/4}$, and $\chi_{1/4}$ with these exponent values. The finite-size scaling for these plots (which we do not present here) is significantly worse than for the scaling plots in Fig. 12. We thus conclude that the tetra-0 to ortho-$\frac{1}{4}$ transition indeed belongs to the universality class of the XY model with cubic anisotropy.

Transfer-matrix data for ν at this transition, obtained with strip widths $M/M' = 4/8$ and $8/12$ at temperatures down to $k_BT \simeq 0.025$, are shown in Fig. 13. Included are also two data points for $M/M' = 12/16$ at $k_BT = 0.15$ and $k_BT \simeq 0.22$. The critical line and ν were determined from the scaling behavior of ξ_1^A, which is the dominant length scale. (An exception is M=12 at temperatures below $k_BT \simeq 0.1$, where the dominant length is ξ_1^S. This case is further discussed below.) The finite-size effects are considerable. At temperatures above $k_BT \simeq 0.13$ the estimates for ν decrease with increasing M, whereas they increase with M below this temperature. Along the portion of the critical line between $\mu \simeq -0.2$ and the multicritical point at $\mu \simeq +0.23$ and $k_BT \simeq 0.222$ the scaling estimates have a wide, flat maximum that decreases with increasing M, reaching $\nu = 0.826$ for $M/M' = 12/16$. There is no indication of a rapid approach to the four-state Potts value of $\nu = \frac{2}{3}$ near the multicritical point, in contrast to the behavior along the tetra-0 to ortho-$\frac{1}{2}$ critical line, where the dominant length is ξ_1^S (see Fig. 7). Around $k_BT \simeq 0.08$ the 8/12 scaling result reaches a broad, shallow minimum of $\nu = 0.67 \pm 0.01$. No dramatic decrease in ν that might indicate a first-order transition is seen at lower temperatures. These numerical results further support the conclusion drawn from the Monte-Carlo simulations described above, that the transition belongs

to the universality class of the XY model with cubic anisotropy. We also find that, although ν depends on temperature, as expected for this universality class, the dependence is rather weak. At $k_BT = 0.15$, the 12/16 scaling of the transfer-matrix data gives $\nu = 0.711$, compared to the best fits presented in Fig. 12, which give $\nu = 0.71$. The transfer-matrix results for ν are thus consistent with those of our detailed Monte Carlo study.

At temperatures below $k_BT \simeq 0.1$, ξ_1^S becomes the dominant length scale for M=12, whereas ξ_1^A remains dominant for M=4 and 8. In this region we also have determined critical points and ν for $M/M' = 8/12$ from scaling of the overall largest length scale, i.e., ξ_1^A for $M = 8$ and ξ_1^S for $M = 12$. Four data points resulting

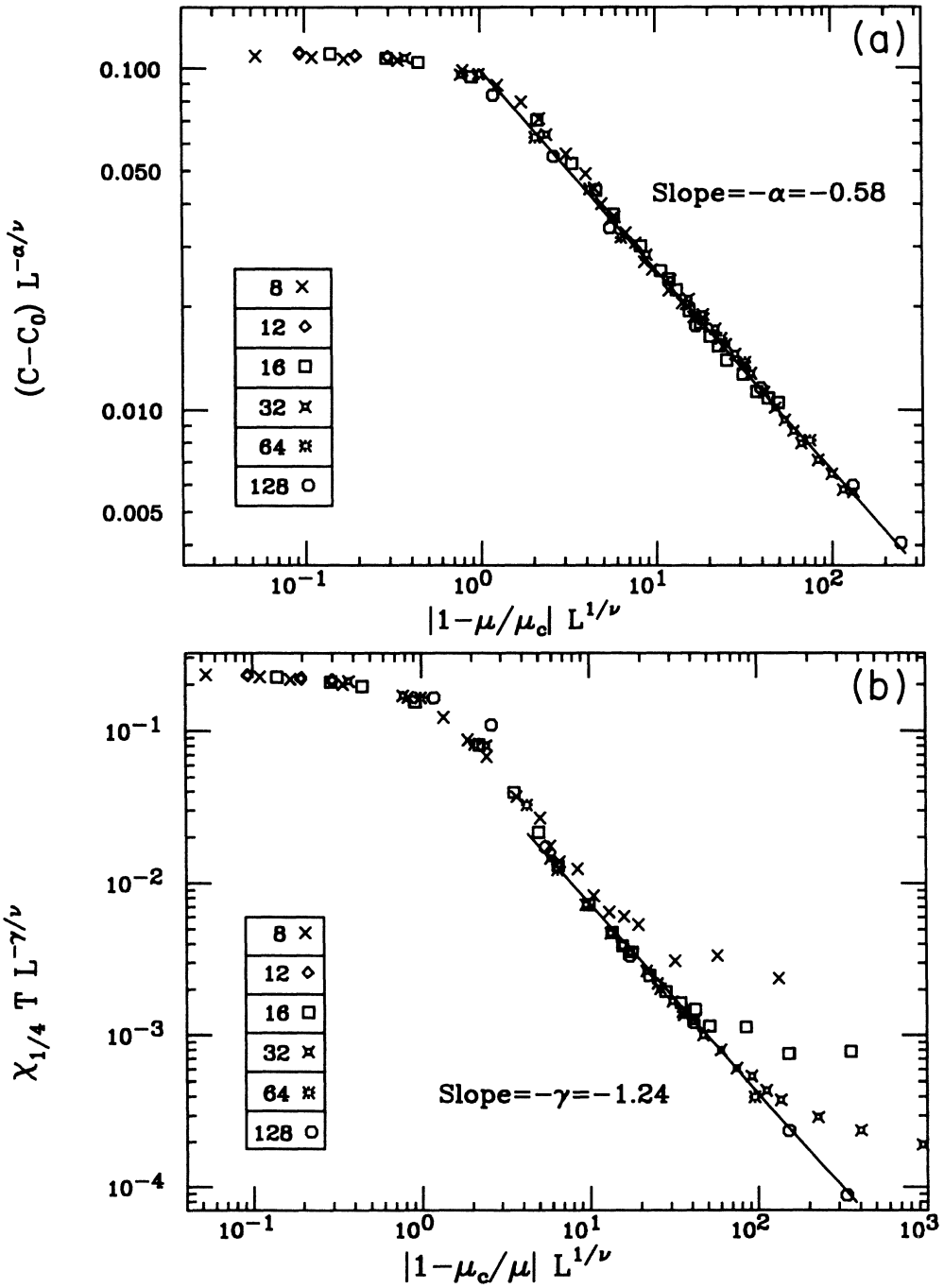

FIG. 12. Finite-size scaling of Monte Carlo data near the disorder to ortho-$\frac{1}{4}$ transition for $k_BT = 0.15$ are shown for (a) the specific heat C and (b) the susceptibility $\chi_{1/4}$ in the ordered phase. The critical exponents used are $\nu = 0.71$, $\alpha = 0.58$, and $\gamma = 1.2425$. We used $\mu_c = -0.4074$ and $C_0 = -0.04$. Only for very large lattice sizes is the asymptotic scaling form of the scaling function obtained.

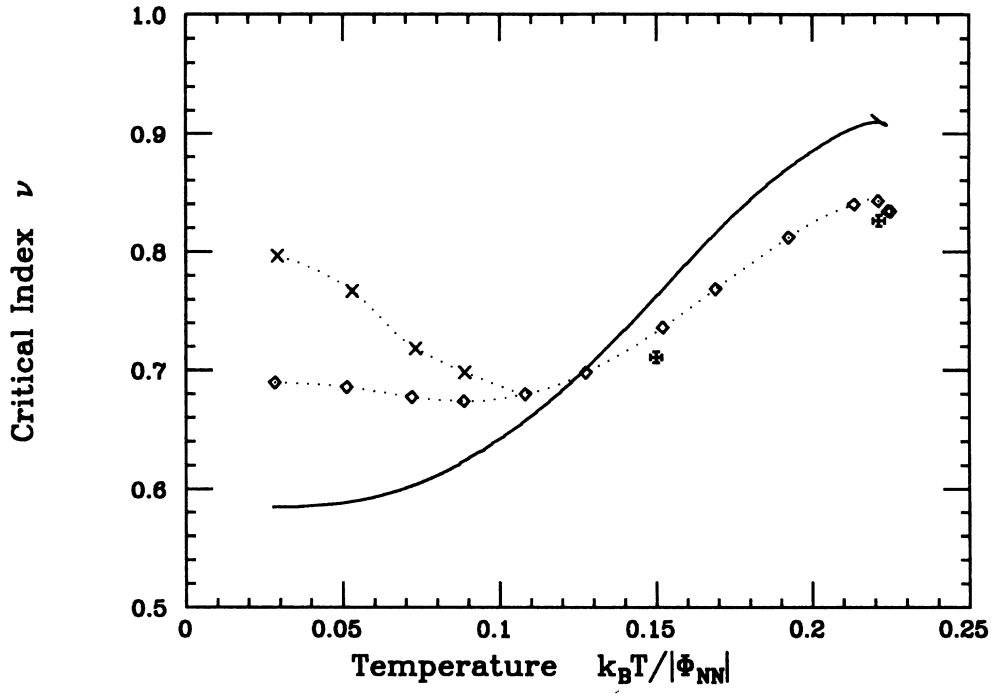

FIG. 13. The critical index ν obtained from transfer-matrix data is shown for the tetra-0 to ortho-$\frac{1}{4}$ transition as a function of temperature. Finite-size scaling results are shown for strip widths 4/8 (solid line), 8/12 ($\times$ or $\diamond$ and the dotted lines), and 12/16 (Roman crosses). (See text for complete description.)

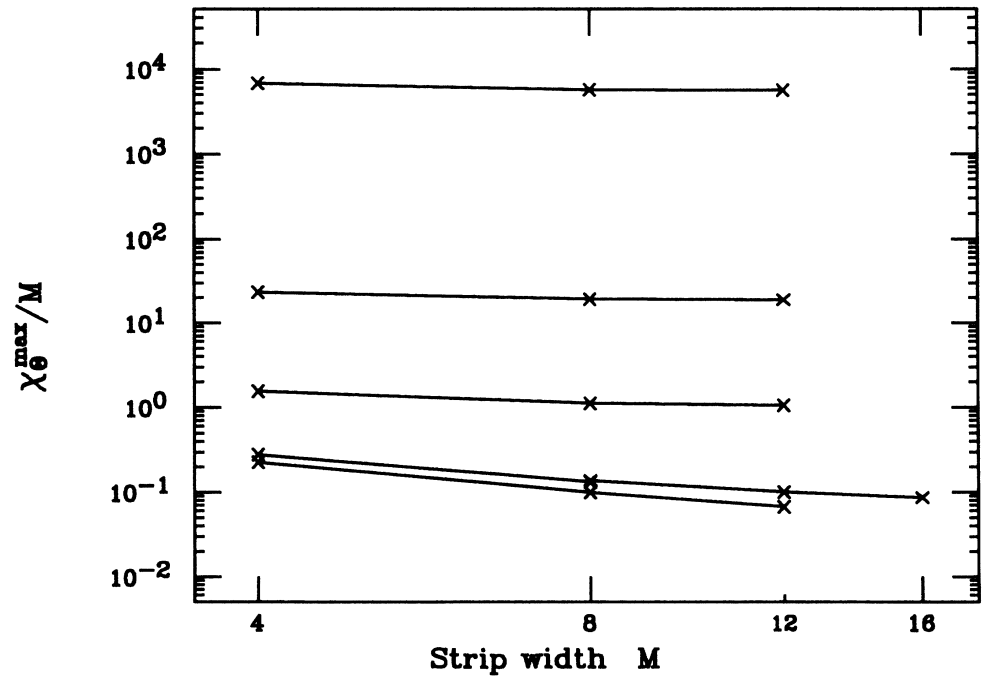

FIG. 14. Scaling plots for the maximum of the nonordering susceptibility χ_Θ^{max} for the tetra-0 to ortho-$\frac{1}{4}$ transition, as obtained from transfer-matrix data are shown. The temperatures are (from below to above in the figure) $k_BT = 0.1625, 0.15, 0.0875, 0.050$, and 0.025. No indication of the exponential growth with M that would signal a first-order transition is seen, even at the lowest temperatures.

from this "mixed" scaling are also shown in Fig. 13. The marked increase in ν with decreasing T is strikingly different from the behavior obtained from the scaling of ξ_1^A. As pointed out in the Appendix, any length scale that contributes to the critical divergence of the susceptibility $\chi_{1/4}$, conjugate to the order parameter $\Theta_{1/4}$, must be among the ξ_α^A. The dominance of ξ_1^S for $M = 12$ at these low temperatures is therefore rather unexpected, and might possibly signal a low-temperature, low oxygen-content phase. This possibility has been suggested by Bartelt *et al.*, based on their independent transfer-matrix calculation,[28] and by Kikuchi and Choi, based on their CVM calculation.[27] However, it is also possible that the transfer-matrix results are due either to subtle finite-size effects, or to numerical errors in the matrix diagonalizations at these low temperatures, where the eigenvalues become nearly degenerate, especially for larger M. The CVM results are suggestive, but in light of the failure of CVM to predict the order of the tetra-0 to ortho-$\frac{1}{4}$ transition correctly, we find them inconclusive. At these low temperatures our Monte Carlo algorithm does not provide useful data, due to the existence of oxygen chains spanning the whole system. Also, our alternative transfer-matrix routine does not converge at low T. On balance, we consider the present numerical evidence for a different ordered phase in this region insufficient. A firm conclusion must await further study.

For this transition, too, we tried to detect a possible first-order transition at low temperatures by searching for hysteresis. We carried out Monte Carlo runs for $L = 64$, starting from the two different ground states corresponding to the ortho-$\frac{1}{4}$ and tetra-0 phases, and scanned μ at fixed temperature. With 2×10^3 MCSS we again find large hysteresis for $k_BT \leq 0.05$. However, at these low temperatures the oxygen chains span the entire lattice. The hysteresis becomes less pronounced as the run length is increased. These observations indicate that the apparent hysteresis most likely is due to large finite-size effects and strong critical slowing-down at a second-order transition, rather than to true metastability associated with a first-order transition.

Figure 14 shows the scaling behavior of the nonordering susceptibility maximum, $\chi_\Theta^{\max}$, discussed in Sec. IVB, at this transition. The strip widths are $M = 4$, 8, and 12 (and $M = 16$ at $k_BT = 0.15$). No indication of the exponential growth with M that would indicate a first-order transition is seen.

The result that the tetra-0 to ortho-$\frac{1}{4}$ transition is second order is in agreement with independent transfer-matrix[28] and Monte Carlo[29,30] calculations, but contradicts the CVM results.[18,27] This discrepancy emphasizes the need to study two-dimensional lattice-gas models of this kind by nonperturbative methods.

VI. DISCUSSION AND CONCLUSIONS

We have presented a comprehensive study by Monte Carlo and transfer-matrix numerical methods of a lattice-gas model for oxygen ordering in the $YBa_2Cu_3O_{6+x}$ high-temperature superconductors. This model was introduced by Wille *et al.*,[18] who also presented a phase diagram based on a calculation by the cluster variation method (CVM). The model describes the formation of oxygen chains in the CuO basal planes, thought to drive the high-temperature tetragonal to orthorhombic phase transition in $RBa_2Cu_3O_{6+x}$ materials (where R is a rare-earth element).

The phase diagrams that we obtain are shown in Figs. 3 and 4. Three lines of continuous phase transitions separate the disordered tetragonal phase with $x \simeq 0$ (corresponding to an oxygen concentration in the Cu-O basal planes of $\Theta \simeq 0$) and two orthogonal phases. One of these latter phases has $x \simeq 0.5$ ($\Theta \simeq 0.25$) and is often referred to as the "double-cell" phase, whereas the other has $x \simeq 1.0$ ($\Theta \simeq 0.5$). For brevity we have denoted the three phases tetra-0, ortho-$\frac{1}{4}$, and ortho-$\frac{1}{2}$, respectively. Our energy scale was adjusted to agree with the transition temperatures obtained by Specht *et al.*[8] from x-ray-diffraction data. The three transition lines meet in a multicritical point at a reduced temperature of $k_BT \simeq 0.22$ (corresponding to approximately 800 K), close to the maximum temperature at which the ortho-$\frac{1}{4}$ phase is stable. We have also included the locations of quasi-one-dimensional disorder lines in the phase diagrams. These disorder lines will be dealt with in greater detail using Monte Carlo and mean-field analysis in a future publication.[62] At high temperatures our phase diagram agrees qualitatively with the CVM results, but at low temperatures there are important differences. Whereas the CVM predicts the tetra-0 to ortho-$\frac{1}{4}$ transition to be first order, both the Monte Carlo and the transfer-matrix calculations clearly indicate that both transitions are second order (continuous), down to at least $k_BT \simeq 0.025$, (approximately 90 K). However, at low temperatures we observe extremely large susceptibilities and strong critical slowing down that without careful finite-size scaling analysis could easily be mistaken for signs of metastability or of first-order transitions. Whether or not first-order transitions occur in the real materials that the model represents is a different question. If, indeed, they do, as some experiments suggest,[67] our results indicate that a more realistic model of the oxygen ordering must include additional effects, such as multi-particle or longer-range interactions, or lattice compressibility. We are currently investigating the phase diagrams of such modified lattice-gas models.[68]

Having established that all the phase transitions in the present model are of second order, we have also performed careful scaling analyses to determine the universality classes of these transitions. We find that the disorder-order tetra-0 to ortho-$\frac{1}{2}$ transition and the order-order ortho-$\frac{1}{4}$ to ortho-$\frac{1}{2}$ transition both belong to the Ising universality class (critical exponents $\nu = 1$, $\beta = \frac{1}{8}$, $\gamma = \frac{7}{4}$). The disorder-order tetra-0 to ortho-$\frac{1}{4}$ transition, on the other hand, belongs to the universality class of the XY model with cubic anisotropy,

which has nonuniversal (variable) critical exponents. In all cases we observe $\gamma/\nu \simeq 1.75$, consistent with Suzuki's weak universality hypothesis.[66] These results agree with Ginzburg-Landau effective free-energy calculations and recent, independent, transfer-matrix calculations.[28] For the same temperatures studied here, the CVM calculation of Kikuchi and Choi[27] and the transfer-matrix calculation of Bartelt *et al.*[28] both give suggestions of an additional orthorhombic phase, intervening between the tetra-0 and ortho-$\frac{1}{4}$ phases at low temperatures. Our transfer-matrix data also show a change in the overall dominant correlation length, from ξ_1^A to ξ_1^S for $N = 12$ at low T. We find this numerical evidence for an additional phase to be inconclusive; it may just as likely be due to subtle finite-size effects, or to numerical difficulties at low temperatures.

We hope that this work provides an impetus for a clear experimental determination of the nature of the phase transition for the tetragonal to "double-cell" structure for $YBa_2Cu_3O_{6+x}$, and, if the transition is continuous, for the determination of the critical exponents. Such experiments would provide valuable information for improved models of oxygen ordering in $YBa_2Cu_3O_{6+x}$.

ACKNOWLEDGMENTS

We thank D. de Fontaine and L. T. Wille for sending us their unpublished results, and L. T. Wille and T. Einstein for useful discussions and for sending us their unpublished independent transfer-matrix calculations.[28] Supported in part by the Florida State University Supercomputer Computations Research Institute, which is partially funded by the U.S. Department of Energy, Contract No. DE-FC05-85ER25000, and by FSU through time granted on its Cyber 205 and ETA-10 supercomputers. M.A.N., P.A.R., and D.P.L. enjoyed the hospitality of the IBM Bergen Scientific Centre. P.A.R. acknowledges partial support by the Donors of the Petroleum Research Fund, administered by the American Chemical Society. D.P.L. acknowledges support from the National Science Foundation Grant No. DMR-8715740.

APPENDIX

We sketch the derivation of the differentiation-free transfer-matrix expression for the thermal eigenvalue $y_T = 1/\nu$. To the best of our knowledge this has not been published elsewhere. For completeness we also give the differentiation-free expression for the nonordering susceptibility χ_Θ that we are using. It is analogous to an expression for the structure factor, obtained by Bartelt and Einstein.[59]

As is well known,[69–72] the moduli of the eigenvalues define quantities, $g_\alpha = -(k_BT/M)\ln|\lambda_\alpha|$, that resemble 'constrained' (nonequilibrium) free energies, in the sense that g_1 is the equilibrium free energy, and their logarithmic field derivatives are related to matrix elements of certain operators. Thus

$$\frac{k_BT}{M}\frac{d}{d\mu}\ln|\lambda_\alpha| = \Re\langle\lambda_\alpha|\Theta|\lambda_\alpha\rangle = \Theta_{\alpha\alpha}\ , \tag{23}$$

where $\Re$ denotes the real part of the matrix element, and the single-layer concentration operator Θ is defined by its matrix elements with the configurations $|X_K\rangle$ of the Kth layer,

$$\langle X_K|\Theta|X_K\rangle = \frac{1}{M}\sum_{m=1}^{M} c_{m,K}. \tag{24}$$

In particular, the equilibrium oxygen concentration, Θ, is $\Theta = \Theta_{11}^S = \langle\lambda_1^S|\Theta|\lambda_1^S\rangle$. (The largest eigenvalue, λ_1^S, is positive, and all elements of its corresponding eigenvectors can be chosen non-negative.) Temperature differentiation is expressed by

$$\begin{aligned}\frac{k_BT}{M}\frac{d}{d(k_BT)}\ln|\lambda_\alpha| &= S_{\alpha\alpha} + \frac{g_\alpha}{k_BT} \\ &= \frac{1}{Mk_BT}\Re\frac{\langle\lambda_\alpha|\mathbf{U}|\lambda_\alpha\rangle}{\lambda_\alpha} - \frac{1}{k_BT}\mu\Theta_{\alpha\alpha} \\ &= \frac{E_{\alpha\alpha}}{k_BT}.\end{aligned} \tag{25}$$

The operator $\mathbf{U}$ is the two-layer internal-energy operator defined by its matrix elements with the configurations $\langle X_K|$ and $|Y_{K+1}\rangle$ of the Kth and $(K+1)$th layers,

$$\langle X_K|\mathbf{U}|Y_{K+1}\rangle = \langle X_K|\mathcal{H}|Y_{K+1}\rangle \exp\left(\frac{-1}{k_BT}\langle X_K|(\mathcal{H}-\mu N_a)|Y_{K+1}\rangle\right) \tag{26}$$

The equilibrium entropy per site (in dimensionless units) is $S = S_{11}^S$, and $E = E_{11}^S$ is the equilibrium expectation value of the Hamiltonian, Eq. (1).

As discussed in Sec. IV B, the thermal eigenvalue, $y_T = \nu^{-1}$, is related to the asymptotic scaling of the gradient $\nabla_{\mathbf{K}}\xi(M)$ of the dominant correlation length with respect to the nonordering fields through Eq. (20). To avoid numerical differentiation we have used the definition $\xi = (\ln|\lambda_1^S/\lambda_\alpha|)^{-1}$, together with Eqs. (23) – (26), to yield the vector

$$\nabla_{\mathbf{K}}\xi(M) = M\xi^2(M)([E(M) - E_{\alpha\alpha}(M)], [\Theta_{\alpha\alpha}(M) - \Theta(M)]). \tag{27}$$

Eqs. (20) and (27), together with the scaling relation for $\xi(M)$ at $\mathbf{K}_C$, Eq. (19), yield the following differentiation-free expression for y_T:

$$y_T \simeq 2 + \left(\ln \frac{\mathbf{v} \cdot ([E(M) - E_{\alpha\alpha}(M)], [\Theta_{\alpha\alpha}(M) - \Theta(M)])}{\mathbf{v} \cdot ([E(M') - E_{\alpha\alpha}(M')], [\Theta_{\alpha\alpha}(M') - \Theta(M')])} \right) \left(\ln \frac{M}{M'} \right)^{-1}. \tag{28}$$

The value of this expression depends on the unit vector in the scaling direction, $\mathbf{v}$. As discussed in Sec. IV B, $\mathbf{v}$ is chosen to minimize this dependence.

For the nonordering susceptibility χ_Θ we use the following expansion in eigenstates of the transfer matrix:

$$\begin{aligned} \chi_\Theta = \frac{M}{k_B T} \Bigg(& \langle \lambda_1^S | \Theta^2 | \lambda_1^S \rangle - \langle \lambda_1^S | \Theta | \lambda_1^S \rangle^2 \\ & + 2 \sum_{\alpha \geq 2} (\langle \lambda_1^S | \Theta | \lambda_\alpha^S R \rangle \langle \lambda_\alpha^S R | \Theta | \lambda_1^S \rangle - \langle \lambda_1^S | \Theta | \lambda_\alpha^S I \rangle \langle \lambda_\alpha^S I | \Theta | \lambda_1^S \rangle) \frac{|\lambda_\alpha^S| (\lambda_1^S \cos\phi_\alpha - |\lambda_\alpha^S|)}{(\lambda_1^S)^2 - 2\lambda_1^S |\lambda_\alpha^S| \cos\phi_\alpha + |\lambda_\alpha^S|^2} \\ & + 2 \sum_{\alpha \geq 2} (\langle \lambda_1^S | \Theta | \lambda_\alpha^S R \rangle \langle \lambda_\alpha^S I | \Theta | \lambda_1^S \rangle + \langle \lambda_1^S | \Theta | \lambda_\alpha^S I \rangle \langle \lambda_\alpha^S R | \Theta | \lambda_1^S \rangle) \frac{|\lambda_\alpha^S| \lambda_1^S \sin\phi_\alpha}{(\lambda_1^S)^2 - 2\lambda_1^S |\lambda_\alpha^S| \cos\phi_\alpha + |\lambda_\alpha^S|^2} \Bigg), \end{aligned} \tag{29}$$

where $\lambda_\alpha = |\lambda_\alpha| e^{i\phi_\alpha}$, $|\lambda_\alpha R\rangle$ and $|\lambda_\alpha I\rangle$ are the real and imaginary parts of the right eigenvectors $|\lambda_\alpha\rangle$, and similarly for the left eigenvectors. The invariance of Θ under the two-step translation operation ensures that the only nonzero matrix elements are those with eigenvectors $|\lambda_\alpha^S\rangle$ of $\mathbf{T^S}$. The sum is performed over *all* eigenstates of $\mathbf{T^S}$, regardless of whether or not the associated eigenvalues belong to a complex conjugate pair.

Analogous expansions for the ordering susceptibilities, $\chi_{1/2}$ and $\chi_{1/4}$, could be constructed. The corresponding single-layer operators, $\Theta_{1/2}$ and $\Theta_{1/4}$, are symmetric and antisymmetric under the two-step translation, respectively. Therefore, the nonzero matrix elements in the expansion of $\chi_{1/2}$ are of the form $\langle \lambda_1^S | \Theta_{1/2} | \lambda_\alpha^S \rangle$. However, the nonzero matrix elements in the expansion of $\chi_{1/4}$ are of the form $\langle \lambda_1^S | \Theta_{1/4} | \lambda_\alpha^A \rangle$, which couples $|\lambda_1^S\rangle$ to the eigenvectors of the antisymmetric block $\mathbf{T^A}$. The divergence of $\chi_{1/4}$ is therefore governed by the largest of the ξ^A.

---

*Author to whom correspondence should be addressed.

[1] J. G. Bednorz and K. A. Müller, Z. Phys. B **64**, 189 (1986).

[2] M. K. Wu, J. R. Ashburn, C. J. Torng, P. H. Hor, R. L. Meng, L. Gao, Z. J. Huang, Y. Q. Wang, and C. W. Chu, Phys. Rev. Lett. **58**, 908 (1987).

[3] A. P. Malozemoff, Physica C **153**, 1049 (1988).

[4] J. D. Jorgensen, M. A. Beno, D. G. Hinks, L. Soderholm, K. J. Volin, R. L. Hitterman, J. D. Grace, I. K. Schuller, C. U. Segre, K. Zhang, and M. S. Kleefisch, Phys. Rev. B **36**, 3608 (1987).

[5] R. J. Cava, B. Batlogg, C. H. Chen, E. A. Rietman, S. M. Zahurak, and D. Weder, Phys. Rev. B **36**, 5719 (1987).

[6] G. Van Tendeloo, H. W. Zandbergen, and S. Amelinckx, Solid State Commun. **63**, 603 (1987).

[7] Y. Kubo, T. Yoshitake, J. Tabuchi, Y. Nakabayashi, A. Ochi, K. Utsumi, H. Igarashi, and M. Yonezawa, Jpn. J. Appl. Phys. **26**, L768 (1987).

[8] E. D. Specht, C. J. Sparks, A. G. Dhere, J. Brynestad, O. B. Cavin, D. M. Kroeger, and H. A. Oye, Phys. Rev. B **37**, 7426 (1988).

[9] F. Beech, S. Miraglia, A. Santoro, and R. S. Roth, Phys. Rev. B **35**, 3608 (1987).

[10] C. H. Chen, D. J. Werder, L. F. Schneemeyer, P. K. Gallagher, and J. V. Waszczak, Phys. Rev. B **38**, 2888 (1988).

[11] H. W. Zandbergen, G. Van Tendeloo, T. Okabe, and S. Amelinckx, Physica Status Solidi A **103**, 45 (1987).

[12] D. de Fontaine, L. T. Wille, and S. C. Moss, Phys. Rev. B **36**, 5709 (1987).

[13] H. Bakker, D. O. Welch, and O. W. Lazareth, Solid State Commun. **64**, 237 (1987).

[14] E. Salomons, N. Koeman, R. Brouwer, D. G. de Groot, and R. Griessen, Solid State Commun. **64**, 1141 (1987).

[15] J. M. Bell, Phys. Rev. B **37**, 541 (1988).

[16] J. M. Sanchez, F. Mejia-Lira, and J. M. Moran-Lopez, Phys. Rev. B **37**, 3678 (1988).

[17] S. B. Ota and T. V. Chandrasekhar Rao, Physica C **153**, 257 (1988).

[18] L. T. Wille, A. Berera, and D. de Fontaine, Phys. Rev. Lett. **60**, 1065 (1988).

[19] A. G. Khachaturyan and J. W. Morris, Jr., Phys. Rev. Lett. **59**, 2776 (1987).

[20] A. G. Khachaturyan and J. W. Morris, Jr., Phys. Rev. Lett. **61**, 215 (1988).

[21] A. G. Khachaturyan, S. V. Semenovskaya, and J. W. Morris, Jr., Phys. Rev. B **37**, 2243 (1988).

[22] L. T. Wille and D. de Fontaine, Phys. Rev. B **37**, 2227 (1988).

[23] A. Berera, L. T. Wille, and D. de Fontaine, J. Stat. Phys. **50**, 1245 (1988).

[24] A. Berera, L. T. Wille, and D. de Fontaine, Physica C **153**, 598 (1988).

[25] L. T. Wille, Phase Trans. (to be published).

[26] R. Beyers and T. Shaw, in *Solid State Physics*, edited by H. Ehrenrich and D. Turnbull (Academic, New York, 1989), Vol. 34, p. 135-212.

[27] R. Kikuchi and J.-S. Choi, Physica C **160**, 347 (1989).

[28] N. C. Bartelt, T. L. Einstein, and L. T. Wille, Phys. Rev. B **40**, 10 759 (1989).

[29] Z.-X. Cai and S. D. Mahanti, Solid State Commun. **67**, 287 (1988); Phys. Rev. B **40**, 6563 (1989).

[30]C. P. Burmester and L. T. Wille, Phys. Rev. B, **40**, 8795 (1989).
[31]E. Domany, M. Schick, J. S. Walker, and R. B. Griffiths, Phys. Rev. B **18**, 2209 (1978).
[32]M. Schick, Prog. Surf. Sci. **11**, 245 (1981).
[33]M. Schick, in *Phase Transitions in Surface Films*, edited by J. G. Dash and J. Ruvalds (Plenum, New York, 1980).
[34]E. Domany and M. Schick, Phys. Rev. B **20**, 3828 (1979).
[35]D. K. Hilton, P. A. Rikvold, and M. A. Novotny (unpublished).
[36]P. Bak, P. Kleban, W. N. Unertl, G. Akinci, N. C. Bartelt, and T. L. Einstein, Phys. Rev. Lett. **54**, 1539 (1985).
[37]D. P. Landau, Phys. Rev. B **13**, 2997 (1976).
[38]D. P. Landau, Phys. Rev. B **14**, 255 (1976).
[39]D. P. Landau, Phys. Rev. B **16**, 4164 (1977).
[40]K. Binder, in *Monte Carlo Methods in Statistical Physics*, edited by K. Binder (Springer, Berlin, 1979).
[41]D. P. Landau, J. Appl. Phys. **42**, 1284 (1971).
[42]K. Binder, Phys. Rev. Lett. **47**, 693 (1981).
[43]K. Binder, Z. Phys. B **43**, 119 (1981).
[44]D. P. Landau and K. Binder, Phys. Rev. B **31**, 5946 (1981).
[45]M. E. Fisher, in Proceedings of the International Summer School "Enrico Fermi" Course 51, Varrena, Italy, 1970, edited by M. S. Green (Academic, New York, 1971), p. 1. p. 1.
[46]M. N. Barber, in *Phase Transitions and Critical Phenomena*, edited by C. Domb and J. L. Lebowitz (Academic, London, 1983), Vol. 8.
[47]A. E. Ferdinand and M. E. Fisher, Phys. Rev. **187**, 832 (1969).
[48]M. A. Novotny, J. Math. Phys. **20**, 1146 (1979).
[49]M. A. Novotny, J. Math. Phys. **29**, 2280 (1988).
[50]J. H. Wilkinson, *The Algebraic Eigenvalue Problem* (Clarendon, Oxford, 1965), p. 607.
[51]M. P. Nightingale, Physica A **83**, 561 (1976).
[52]M. P. Nightingale, Phys. Lett. **59A**, 486 (1977).
[53]M. N. Barber, Phys. Rev. B **27**, 5879 (1983).
[54]P. A. Rikvold, W. Kinzel, J. D. Gunton, and K. Kaski, Phys. Rev. B **28**, 2686 (1983).
[55]P. A. Rikvold, K. Kaski, J. D. Gunton, and M. C. Yalabik, Phys. Rev. B **29**, 6285 (1984).
[56]J. B. Collins, P. A. Rikvold, and E. T. Gawlinski, Phys. Rev. B **38**, 6741 (1988).
[57]P. A. Rikvold, Phys. Rev. B **32**, 4756 (1985).
[58]P. A. Rikvold, Phys. Rev. B **33**, 6523 (1986).
[59]N. C. Bartelt and T. L. Einstein, J. Phys. A **19**, 1429 (1986).
[60]W. R. McKinnon, M. L. Post, L. S. Selwyn, G. Pleizier, J. M. Tarascon, P. Barboux, L. H. Greene, and G. W. Hull, Phys. Rev. B **38**, 6543 (1988).
[61]D. de Fontaine, M. E. Mann, and G. Ceder, Phys. Rev. Lett. **63**, 1300 (1989).
[62]P. A. Rikvold, M. A. Novotny, and T. Aukrust (unpublished).
[63]M. A. Novotny and D. P. Landau, Phys. Rev. B **24**, 1468 (1981).
[64]R. H. Swendsen, in *Real Space Renormalization* , edited by T. W. Burkhardt and J. M. J. van Leeuwen (Springer, New York, 1982).
[65]B. Nienhuis, A. N. Berker, E. K. Riedel, and M. Schick, Phys. Rev. Lett. **43**, 737 (1979).
[66]M. Suzuki, Prog. Theor. Phys. **51**, 1992 (1974).
[67]H. You, J. D. Axe, X. B. Kan, S. Hashimoto, S. C. Moss, J. Z. Liu, G. W. Crabtree, and D. J. Lam, Phys. Rev. B **38**, 9213 (1988).
[68]C. C. A. Günther, P. A. Rikvold, and M. A. Novotny (unpublished).
[69]V. Privman and L. S. Schulman, J. Phys. A **15**, L231 (1982).
[70]V. Privman and L. S. Schulman, J. Stat. Phys. **31**, 205 (1982).
[71]M. A. Novotny, W. Klein, and P. A. Rikvold, Phys. Rev. B **33**, 7729 (1986).
[72]P. A. Rikvold, Prog. Theor. Phys. (to be published).